CHAPTER VI

EXPERIMENTAL FLOW IN TWO-DIMENSIONAL CASCADES

By SEYMOUR LIEBLEIN

Available experimental two-dimensional-cascade data for conventional compressor blade sections are correlated. The two-dimensional cascade and some of the principal aerodynamic factors involved in its operation are first briefly described. Then the data are analyzed by examining the variation of cascade performance at a reference incidence angle in the region of minimum loss. Variations of reference incidence angle, total-pressure loss, and deviation angle with cascade geometry, inlet Mach number, and Reynolds number are investigated.

From the analysis and the correlations of the available data, rules and relations are evolved for the prediction of the magnitude of the reference total-pressure loss and the reference deviation and incidence angles for conventional blade profiles. These relations are developed in simplified forms readily applicable to compressor design procedures.

INTRODUCTION

Because of the complexity and three-dimensional character of the flow in multistage axial-flow compressors, various simplified approaches have been adopted in the quest for accurate blade-design data. The prevailing approach has been to treat the flow across individual compressor blade sections as a two-dimensional flow. The use of two-dimensionally derived flow characteristics in compressor design has generally been satisfactory for conservative units (ch. III).

In view of the limitations involved in the theoretical calculation of the flow about two-dimensional blade sections (chs. IV and V), experimental investigations of two-dimensional cascades of blade sections were adopted as the principal source of blade-design data. Early experimental cascade results (e.g., refs. 184 to 186), however, were marked by a sensitivity to individual tunnel design and operation. This was largely a result of the failure to obtain true two-dimensional flow. Under these circumstances, the correlation of isolated data was very difficult. Some efforts were made, however, to correlate limited experimental data for use in compressor design (e.g., ref. 187). The British, in particular, through the efforts primarily of Carter and Howell, appear to have made effective use of their early cascade investigations (refs. 31 (pt. I) and 188 to 190).

In recent years, the introduction of effective tunnel-wall boundary-layer removal for the establishment of true two-dimensional flow gave a substantial impetus to cascade analysis. In particular, the porous-wall technique of boundary-layer removal developed by the NACA (ref. 191) was a notable contribution. The use of effective tunnel boundary-layer control has resulted in more consistent systematic test data (refs. 39, 54, 123, and 192 (pt. II)) and in more significant two-dimensional comparisons between theoretical and experimental performance (refs. 98, 167 (pt. I), and 193). With the availability of a considerable amount of consistent data, it has become feasible to investigate the existence of general relations among the various cascade flow parameters. Such relations curtail the amount of future experimental data needed and also result in more effective use of the data currently available.

Since the primary function of cascade information is to aid in the design of compressors, the present chapter expresses the existing cascade data in terms of parameters applicable to compressor design. Such expression not only facilitates the design of moderate compressors but also makes possible a rapid comparison of cascade data with data obtained from advanced high-speed compressor configurations. Since the bulk of the available cascade data has been obtained at low speed (Mach numbers of the order of 0.1), the question of applicability to such high-speed units is very significant. It is necessary to determine which flow parameters can or cannot be applied,

to what extent the low-speed data are directly usable, and whether corrections can be developed in those areas where the low-speed data cannot be used directly.

In this chapter, the available cascade data obtained from a large number of tunnels are reworked in terms of what are believed to be significant parameters and are correlated in generalized forms wherever possible. The performance parameters considered in the correlation are the outlet-air deviation angle and the cascade losses expressed in terms of blade-wake momentum thickness. The correlations are based on the variations of the performance parameters with cascade geometry (blade profile shape, solidity, chord angle) and inlet flow conditions. In view of the difficulties involved in establishing correlations over the complete range of operation of the cascade at various Mach number levels, the analysis is restricted to an examination of cascade performance at a reference incidence-angle location in the region of minimum loss.

The chapter is divided into four main sections: (1) a brief description of the two-dimensional cascade and of the parameters, concepts, and data involved in the analysis; (2) an analysis of the variation of the reference incidence angle with cascade geometry and flow conditions; (3) an analysis of the variation of total-pressure loss at the reference incidence angle; and (4) an analysis of the variation of deviation angle at the reference incidence angle.

SYMBOLS

The following symbols are used in this chapter:

A	flow area
b	exponent in deviation-angle relation
c	chord length
D	diffusion factor (based on over-all velocities)
D_{loc}	local diffusion factor (based on local velocities)
d	exponent in wake velocity-distribution relations
f	function
H	wake form factor, δ^*/θ^*
i	incidence angle, angle between inlet-air direction and tangent to blade mean camber line at leading edge, deg
i_o	incidence angle of uncambered blade section, deg
K_c	compressibility correction factor in loss equation
K_i	correction factor in incidence-angle relation
K_s	correction factor in deviation-angle relation
M	Mach number
m, m_c	factors in deviation-angle relation
n	slope factor in incidence-angle relation
P	total or stagnation pressure
p	static or stream pressure
Re_c	Reynolds number based on chord length
s	blade spacing
t	blade maximum thickness
V	air velocity
y	coordinate normal to axis
z	coordinate along axis
α	angle of attack, angle between inlet-air direction and blade chord, deg
β	air angle, angle between air velocity and axial direction, deg
$\Delta\beta$	air-turning angle, $\beta_1-\beta_2$, deg
γ°	blade-chord angle, angle between blade chord and axial direction, deg
δ	wake full thickness
δ^*	wake displacement thickness
δ°	deviation angle, angle between outlet-air direction and tangent to blade mean camber line at trailing edge, deg
δ_o°	deviation angle of uncambered blade section, deg
θ^*	wake momentum-defect thickness
κ	blade angle, angle between tangent to blade mean camber line and axial direction, deg
ρ	density
σ	solidity, ratio of chord to spacing
φ	blade camber angle, difference between blade angles at leading and trailing edges, $\kappa_1-\kappa_2$, deg
$\overline{\omega}$	total-pressure-loss coefficient

Subscripts:

av	average
$i.e.$	incompressible equation
inc	incompressible
l	lower surface
max	maximum
min	minimum
ref	reference

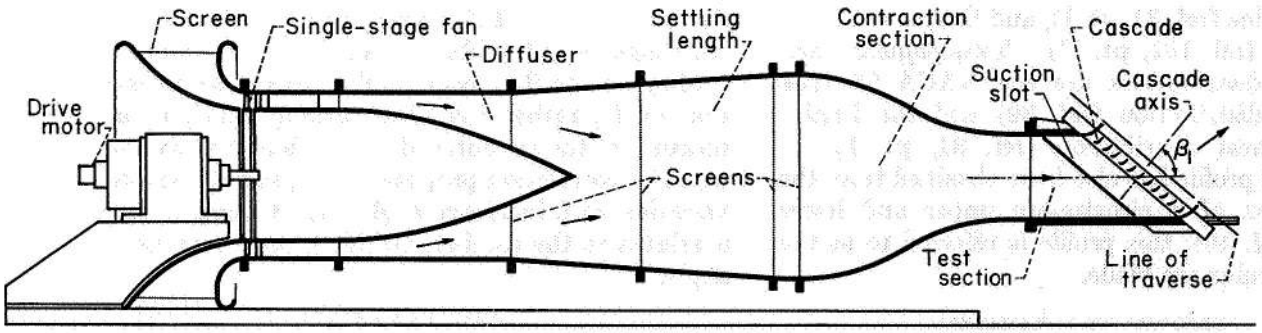

FIGURE 123.—Layout of conventional low-speed cascade tunnel (ref. 168).

sh	blade shape
t	blade maximum thickness
u	upper surface
z	axial direction
θ	tangential direction
0	free stream
1	station at cascade inlet
2	station at cascade exit (measuring station)
10	10 percent thick

PRELIMINARY CONSIDERATIONS

DESCRIPTION OF CASCADE

A schematic diagram of a low-speed two-dimensional-cascade tunnel is shown in figure 123 to illustrate the general tunnel layout. The principal components of the conventional tunnel are a blower, a diffuser section, a large settling chamber with honeycomb and screens to remove any swirl and to ensure a uniform velocity distribution, a contracting section to accelerate the flow, the cascade test section, and some form of outlet-air guidance. The test section contains a row or cascade of blades set in a mounting device that can be altered to obtain a range of air inlet angles (angle β_1 in figs. 123 and 124). Variations in blade angle of attack are obtained either by rotating the blades on their individual mounting axes (i.e., by varying the blade-chord angle $\gamma°$) while maintaining a fixed air angle or by keeping the blade-chord angle fixed and varying the air inlet angle by rotating the entire cascade. Outlet flow measurements are obtained from a traverse along the cascade usually between $\frac{1}{2}$ and $1\frac{1}{2}$ chord lengths behind the blade trailing edge at the blade midspan. In the analysis, blade outlet refers to the cascade measuring station.

In most cases, some form of wall boundary-layer control in the cascade is provided by means of suction through slots or porous-wall surfaces. Examples of different tunnel designs or detailed information concerning design, construction, and operation of the two-dimensional-cascade tunnel can be obtained from references 39, 122, 168, 191, and 194.

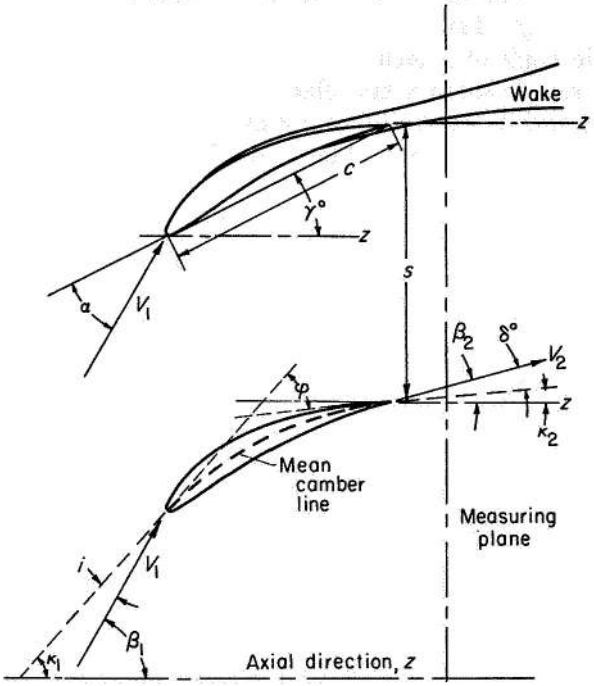

FIGURE 124.—Nomenclature for cascade blade.

Nomenclature and symbols designating cascade blade characteristics are given in figure 124. As in isolated-airfoil practice, cascade blade shapes are normally evolved by adding a basic thickness distribution to a mean camber line. The mean camber line (as indicated in fig. 124) represents the basic curvature of the profile. Some frequently used curvatures are the NACA (A_{10}) and related mean lines (refs. 39 and 123), the circular-

arc mean line (ref. 31, pt. I), and the parabolic-arc mean line (ref. 192, pt. II). Two popular basic thickness distributions are the NACA 65-series thickness distribution (ref. 39) and the British C.4 thickness distribution (ref. 31, pt. I). A high-speed profile has also been obtained from the construction of a circular-arc upper and lower surface (ref. 40); this profile is referred to as the double-circular-arc blade.

PERFORMANCE PARAMETERS

The performance of cascade blade sections has generally been presented as plots of the variation of air-turning angle, lift coefficient, and flow losses against blade angle of attack (or incidence angle) for a given cascade solidity and blade orientation. Blade orientation is expressed in terms of either fixed air inlet angle or fixed blade-chord angle. Flow losses have been expressed in terms of coefficients of the drag force and the defects in outlet total pressure or momentum. A recent investigation (ref. 156) demonstrates the significance of presenting cascade losses in terms of the thickness and form characteristics of the blade wakes.

In this analysis, the cascade loss parameters considered are the wake momentum-thickness ratio θ^*/c (ref. 156) and the total-pressure-loss coefficient $\bar{\omega}_1$, defined as the ratio of the average loss in total pressure across the blade to the inlet dynamic head. Cascade losses are considered in terms of $\bar{\omega}_1$, since this parameter can be conveniently used for the determination of compressor blade-row efficiency and entropy gradients. The parameter θ^*/c represents the basic wake development of the blade profile and as such constitutes a significant parameter for correlation purposes. Values of θ^*/c were computed from the cascade loss data according to methods similar to those presented in reference 156. The diffusion factor D of reference 9 was used as a measure of the blade loading in the region of minimum loss.

In the present analysis, it was necessary to use a uniform nomenclature and consistent correlation technique for the various blade shapes considered. It was believed that this could best be accomplished by considering the approach characteristics of the blade in terms of air incidence angle i, the camber characteristics in terms of the camber angle φ, and the air-turning characteristics in terms of the deviation angle δ° (fig. 124). As indicated in figure 124, these angles are based on the tangents to the blade mean camber line at the leading and trailing edges. The use of the deviation angle, rather than the turning angle, as a measure of the air outlet direction has the advantage, for correlation purposes, of a generally small variation with incidence angle. Air-turning angle is related to the camber, incidence, and deviation angles by

$$\Delta\beta=\varphi+i-\delta^\circ \tag{57}$$

Incidence angle is considered positive when it tends to increase the air-turning angle, and deviation angle is considered positive when it tends to decrease the air-turning angle (fig. 124).

The use of incidence and deviation angles requires a unique and reasonable definition of the blade mean-line angle at the leading and trailing edges, which may not be possible for some blade shapes. The principal difficulty in this respect is in the 65-(A_{10})-series blades (ref. 39), whose mean-line slope is theoretically infinite at the leading and trailing edges. However, it is still possible to render these sections usable in the analysis by arbitrarily establishing an equivalent circular-arc mean camber line. As shown in figure 125, the equivalent circular-arc mean line is obtained by drawing a circular arc through the leading- and trailing-edge points and the point of maximum camber at the midchord position. Equivalent incidence, deviation, and camber angles can then be established from the equivalent circular-arc mean line as indicated in the figure. The relation between equivalent camber angle and isolated-airfoil lift coefficient of the NACA 65-(A_{10})-series mean line is shown in figure 126.

A typical plot of the cascade performance parameters used in the analysis is shown in figure 127 for a conventional blade section at fixed solidity and air inlet angle.

DATA SELECTION

In selecting data sources for use in the cascade performance correlations, it is necessary to consider the degree of two-dimensionality obtained in the tunnel and the magnitude of the test Reynolds number and turbulence level.

Two-dimensionality.—As indicated previously, test results for a given cascade geometry obtained from different tunnels may vary because of a fail-

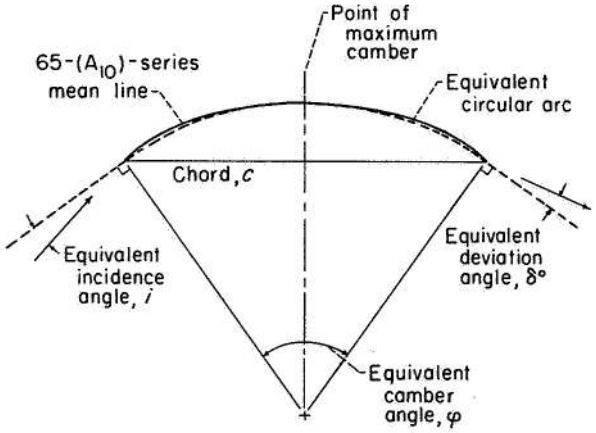

FIGURE 125.—Equivalent circular-arc mean line for NACA 65-(A_{10})-series blades.

ure to achieve true two-dimensional flow across the cascade. Distortions of the true two-dimensional flow are caused by the tunnel-wall boundary-layer growth and by nonuniform inlet and outlet flow distributions (refs. 191 and 168). In modern cascade practice, good flow two-dimensionality is obtained by the use of wall-boundary-layer control or large tunnel size in conjunction with a large number of blades, or both. Examples of cascade tunnels with good two-dimensionality are given by references 39 and 194.

The lack of good two-dimensionality in cascade testing affects primarily the air-turning angles and blade surface pressure distributions. Therefore, deviation-angle data were rejected when the two-dimensionality of the tunnel appeared questionable (usually the older and smaller tunnels). Practically all the cascade loss data were usable, however, since variations in the measured loss obtained from a given cascade geometry in different tunnels will generally be consistent with the measured diffusion levels (unless the blade span is less than about 1 or 2 inches and there is no extensive boundary-layer removal).

Reynolds number and turbulence.—For the same conditions of two-dimensionality and test-section Mach number, test results obtained from cascades of the same geometry may vary because of large differences in the magnitude of the bladechord Reynolds number and the free-stream turbulence. Examples of the effect of Reynolds number and turbulence on the losses obtained from a given blade section at fixed incidence angle are presented in figure 128. Similar pronounced effects are observed on the deviation angle. As discussed in chapter V, the loss variation with Reynolds number is associated primarily with a local or complete separation of the laminar boundary layer on the blade surfaces. The data used in the correlation are restricted to values of blade-chord Reynolds number from about 2.0×10^5 to 2.5×10^5 in order to minimize the effects of different Reynolds numbers. Free-stream turbulence level was not generally determined in the various cascade tunnels.

In some cases (refs. 39 and 195, e.g.), in tunnels with low turbulence levels, marked local laminar-separation effects were observed in the range of Reynolds number selected for the correlation. Illustrative plots of the variation of total-pressure-loss coefficient with angle of attack for a cascade with local laminar separation are shown in figure 129. In such instances, it was necessary to estimate the probable variation of loss (and deviation angle) in the absence of the local separation (as indicated in the figure) and use values obtained from the faired curves for the correlations.

The specific sources of data used in the analysis are indicated by the references listed for the various performance correlations. Details of the tunnel construction and operation and other pertinent information are given in the individual references.

APPROACH

In a correlation of two-dimensional-cascade data that is intended ultimately for use in compressor blade-element design, the variations of performance parameters should be established over a wide range of incidence angles. Experience shows (fig. 130) that the variation of loss with incidence angle for a given blade section changes markedly as the inlet Mach number is increased. Consequently, correlated low-speed blade performance at high and low incidence angles is not applicable at high Mach numbers. The low-speed-cascade performance is therefore considered at some reference point on the general loss-against-incidence-angle curve that exhibits the least variation in location and in magnitude of performance parameters as Mach number is increased.

The reference location herein is selected as the point of minimum loss on the curve of total-

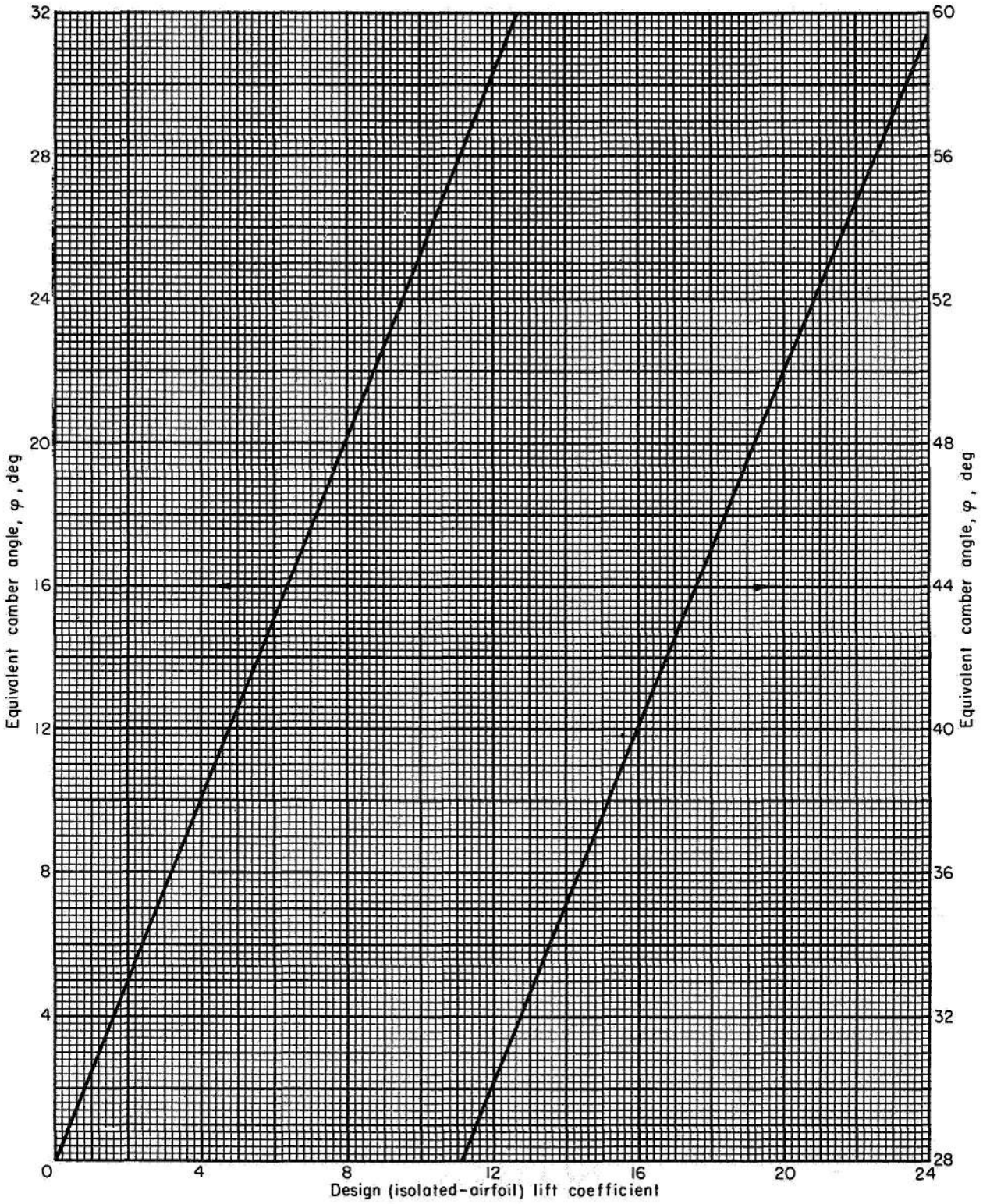

FIGURE 126.—Equivalent camber angles for NACA 65-($C_{l_0}A_{10}$) mean camber line as equivalent circular arc (fig. 125).

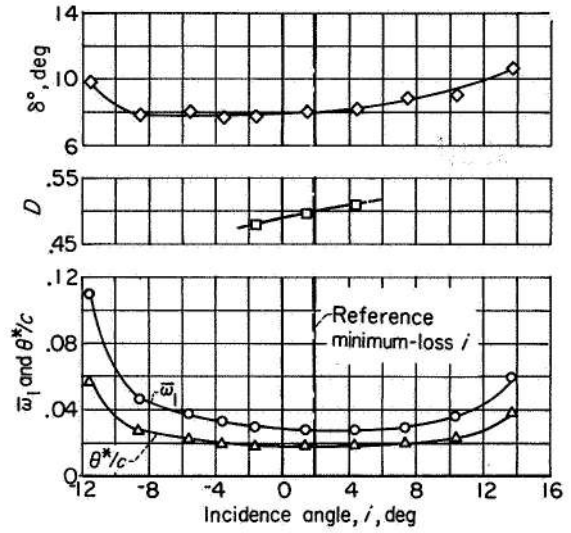

FIGURE 127.—Illustration of basic performance parameters for cascade analysis. Data obtained from conventional blade geometry in low-speed two-dimensional tunnel.

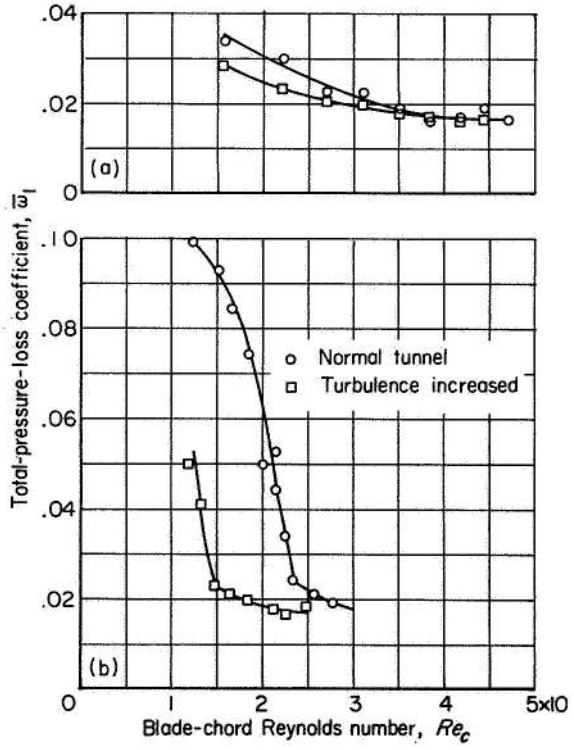

(a) NACA 65–(12)10 blade. Inlet-air angle, 45°; solidity, 1.5 (ref.39):
(b) Lighthill blade, 50 percent laminar flow. Inlet-air angle, 45.5°; solidity, 1.0 (ref. 167, pt. I).

FIGURE 128.—Effect of blade-chord Reynolds number and free-stream turbulence on minimum-loss coefficient of cascade blade section in two-dimensional tunnel.

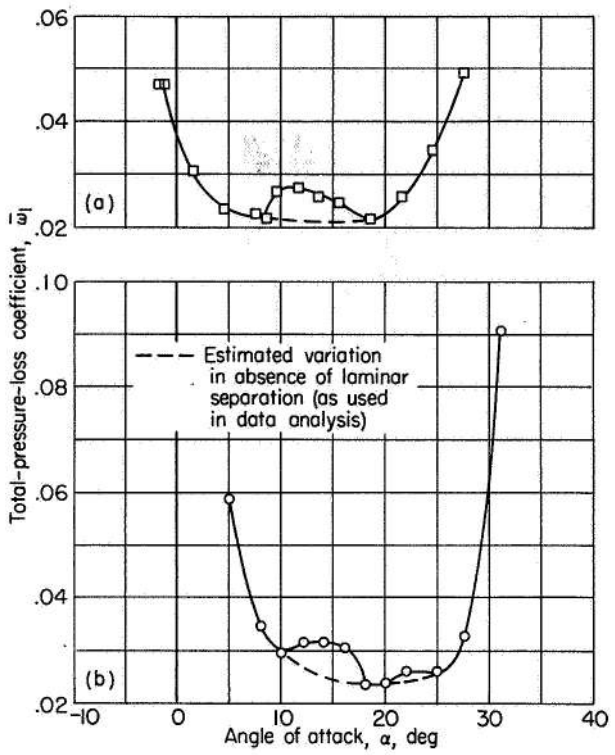

(a) NACA 65–810 blade. Inlet-air angle, 30°.
(b) NACA 65–(12)10 blade. Inlet-air angle, 45°.

FIGURE 129.—Loss characteristics of cascade blade with local laminar separation. Solidity, 1.5; blade-chord Reynolds number, 2.45×10^5 (ref. 39).

pressure loss against incidence angle. For conventional low-speed-cascade sections, the region of low-loss operation is generally flat, and it is difficult to establish precisely the value of incidence angle that corresponds to the minimum loss. For practical purposes, therefore, since the curves of loss coefficient against incidence angle are generally symmetrical, the reference minimum-loss location was established at the middle of the low-loss range of operation. Specifically, as shown in figure 131, the reference location is selected as the incidence angle at the midpoint of the range, where range is defined as the change in incidence angle corresponding to a rise in loss coefficient equal to the minimum value. Thus, for conventional cascade sections, the midrange reference location is considered coincident with the point of minimum loss. In addition to meeting the abovementioned requirement of small variation with inlet Mach number, the reference minimum-loss incidence

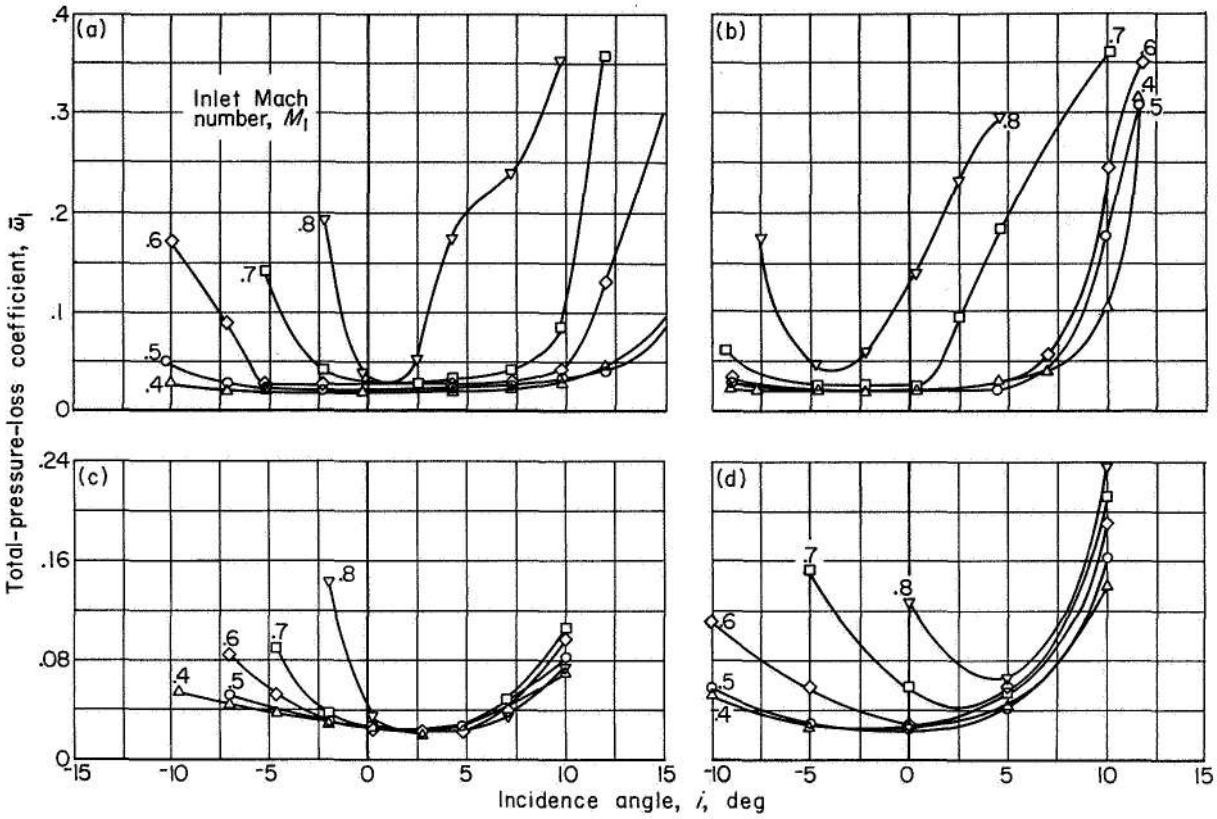

(a) C.4 Circular-arc blade. Camber angle, 25°; maximum-thickness ratio, 0.10; solidity, 1.333; blade-chord angle, 42.5° (ref. 40). (b) C.4 Parabolic-ard blade. Camber angle, 25°; maximum-thickness ratio, 0.10; solidity, 1.333; blade-chord angle, 37.6° (ref. 40). (c) Double-circular-arc blade. Camber angle, 25°; maximum-thickness ratio, 0.105; solidity, 1.333; blade-chord angle, 42.5° (ref. 40). (d) Sharp-nose blade. Camber angle, 27.5°; maximum-thickness ratio, 0.08; solidity, 1.15; blade-chord angle, 30° (ref. 205).

FIGURE 130.—Effect of inlet Mach number on loss characteristics of cascade blade sections.

angle (as compared with the optimum or nominal incidence settings of ref. 196 or the design incidence setting of ref. 39) requires the use of only the loss variation and also permits the use of the diffusion factor (applicable in region of minimum loss) as a measure of the blade loading.

At this point, it should be kept in mind that the reference minimum-loss incidence angle is not necessarily to be considered as a recommended design point for compressor application. The selection of the best incidence angle for a particular blade element in a multistage-compressor design is a function of many considerations, such as the location of the blade row, the design Mach number, and the type and application of the design. In general, there is no one universal definition of design or best incidence angle. The cascade

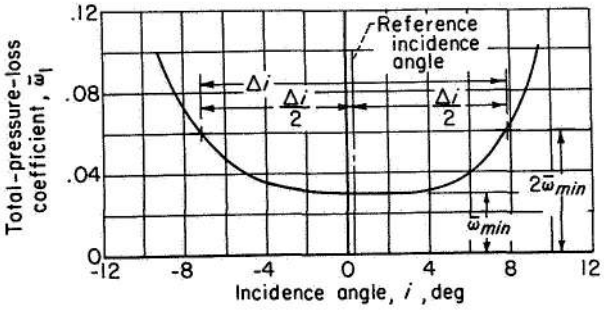

FIGURE 131.—Definition of reference minimum-loss incidence angle.

reference location is established primarily for purposes of analysis.

Of the many blade shapes currently in use in compressor design practice (i.e., NACA 65-series, C-series circular arc, parabolic arc, double

circular arc), data sufficient to permit a reasonably complete and significant correlation have been published only for the 65-(A_{10})-series blades of reference 39. Therefore, a basic correlation of the 65-(A_{10})-series data had to be established first and the results used as a guide or foundation for determining the corresponding performance trends for the other blade shapes for which only limited data exist.

Since the ultimate objective of cascade tests is to provide information for designing compressors, it is desirable, of course, that the structure of the data correlations represent the compressor situation as closely as possible. Actually, a blade element in a compressor represents a blade section of fixed geometry (i.e., fixed profile form, solidity, and chord angle) with varying inlet-air angle. In two-dimensional-cascade practice, however, variations in incidence angle have been obtained by varying either the inlet-air angle or the blade-chord angle. The available systematic data for the NACA 65-(A_{10})-series blades (ref. 39) have been obtained under conditions of fixed inlet-air angle and varying blade-chord angle. Since these data form the foundation of the analysis, it was necessary to establish the cascade performance correlations on the basis of fixed inlet-air angle. Examination of limited unpublished low-speed data indicate that, as illustrated in figure 132, the loss curve for constant air inlet angle generally falls somewhat to the right of the constant-chord-angle curve for fixed values of β_1 and $\gamma°$ in the low-loss region of the curve. Values of minimum-loss incidence angle for fixed β_1 operation are indicated to be of the order of 1° or 2° greater than for fixed $\gamma°$ operation. An approximate allowance for this difference is made

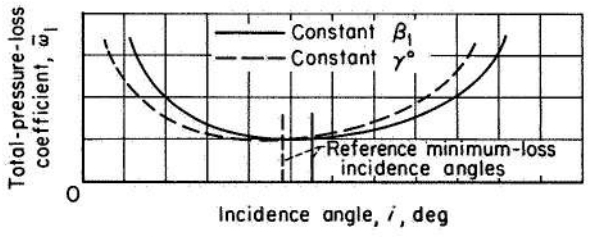

FIGURE 132.—Qualitative comparison of cascade range characteristics at constant blade-chord angle and constant inlet-air angle (for same value of β_1 in region of minimum loss).

in the use of reference-incidence-angle data from these two methods.

With the definition of reference incidence angle, performance parameters, and analytical approach established, the procedure is first to determine how the value of the reference minimum-loss incidence angle varies with cascade geometry and flow conditions for the available blade profiles. Then the variation of the performance parameters is determined at the reference location (as indicated in fig. 127) as geometry and flow are changed. Thus, the various factors involved can be appraised, and correlation curves and charts can be established for the available data. The analysis and correlation of cascade reference-point characteristics are presented in the following sections.

INCIDENCE-ANGLE ANALYSIS

PRELIMINARY ANALYSIS

In an effort to obtain a general empirical rule for the location of the reference minimum-loss incidence angle, it is first necessary to examine the principal influencing factors.

It is generally recognized that the low-loss region of incidence angle is identified with the absence of large velocity peaks (and subsequent decelerations) on either blade surface. For infinitely thin sections, steep velocity gradients are avoided when the front stagnation point is located at the leading edge. This condition has frequently been referred to as the condition of "impact-free entry." Weinig (ref. 80) used the criterion of stagnation-point location to establish the variation of impact-free-entry incidence angle for infinitely thin circular-arc sections from potential-flow theory. Results deduced from reference 80 are presented in figure 133(a). The minimum-loss incidence angle is negative for infinitely thin blades and decreases linearly with camber for fixed solidity and blade-chord angle.

While there is no definite corresponding i-inc dence-angle theory for thick-nose blades with rounded leading edges, some equivalent results have been obtained based on the criterion that the location of the stagnation point in the leading-edge region of a thick blade is the controlling factor in the determination of the surface velocity distributions. Carter, in reference 190, showed semitheoretically on this basis that optimum incidence angle (angle at maximum lift-drag ratio)

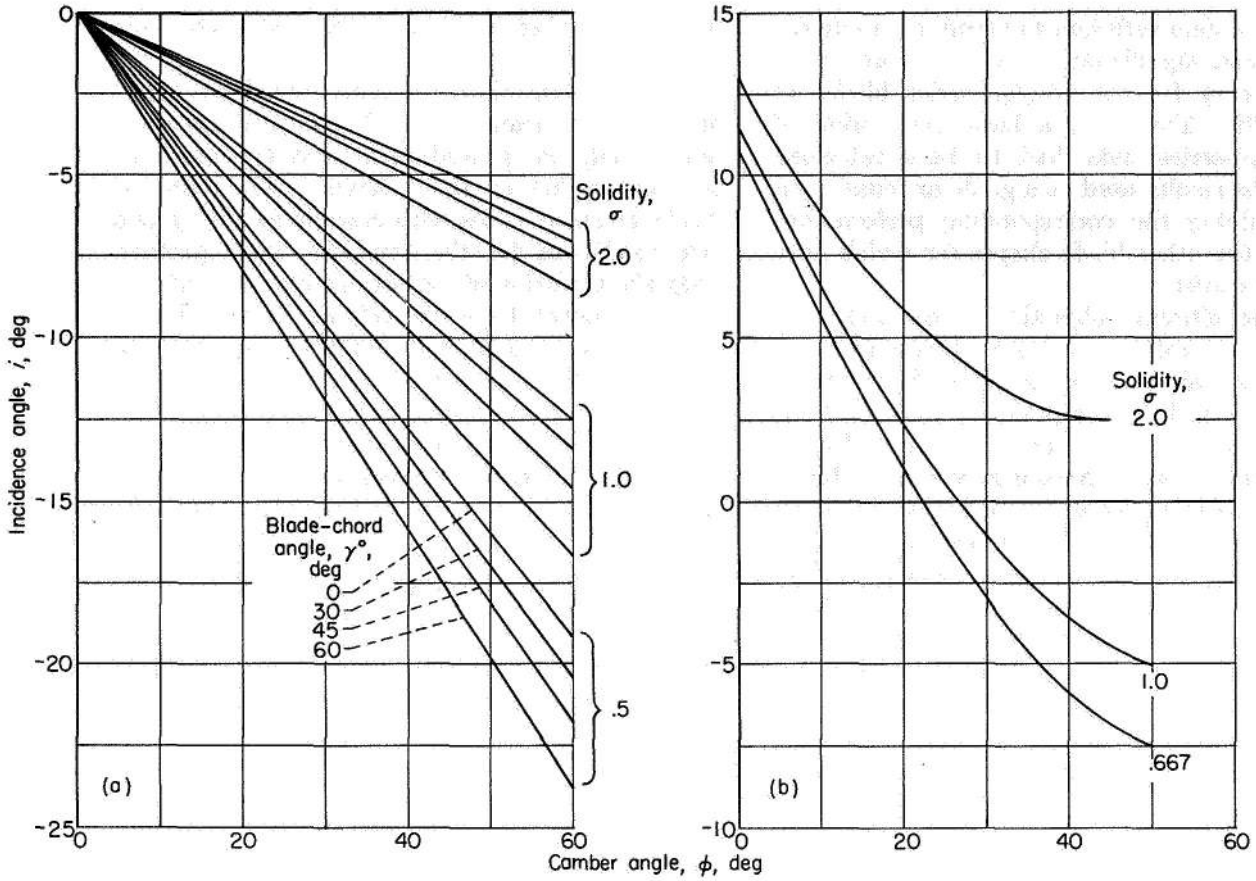

(a) "Impact-free-entry" incidence angle for infinitely thin blades according to potential theory of Weinig (ref. 80).
(b) "Optimum" incidence angle for 10-percent-thick C-series profiles according to semitheoretical developments of Carter *et al.* (refs. 190 and 196). Outlet-air angle, 20°.

FIGURE 133.—Variation of reference incidence angle for circular-air-mean-line blades obtained from theoretical or semitheoretical investigations.

for a conventional 10-percent-thick circular-arc blade decreases with increasing camber angle. The results of reference 190 were followed by generalized plots of optimum incidence angle in reference 196, which showed, as in figure 133(a), that optimum incidence angle for a 10-percent-thick C-series blade varies with camber angle, solidity, and blade orientation. (In these references, blade orientation was expressed in terms of air outlet angle rather than blade-chord angle.) The plot for an outlet-air angle of 20° is shown in figure 133(b). Apparently, the greater the blade circulation, the lower in magnitude the minimum-loss incidence angle must be. It is reasonable to expect, therefore, that the trends of variation of minimum-loss incidence angle for conventional blade sections will be similar to those established by thin-airfoil theory.

A preliminary examination of experimental cascade data showed that the minimum-loss incidence angles of uncambered sections ($\phi=0$) of conventional thicknesses were not zero, as indicated by theory for infinitely thin blades (fig. 133(a)), but always positive in value. The appearance of positive values of incidence angle for thick blades is attributed to the existence of velocity distributions at zero incidence angle that are not symmetrical on the two surfaces. Typical plots illustrating the high velocities generally observed in the inlet region of the lower (pressure) surface of thick uncambered blades at zero incidence angle are shown in figure 134. Apparently, an increase in incidence angle from the zero value is necessary in order to reduce the lower-surface velocity to a more equitable distribution that results in a minimum of the over-all loss. This

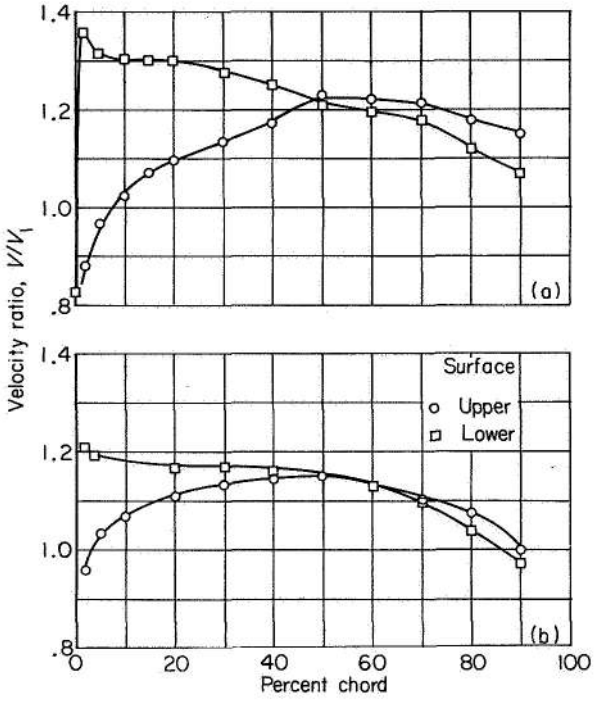

(a) Inlet-air angle, 60°; solidity, 1.5.
(b) Inlet-air angle, 30°; solidity, 1.0.

FIGURE 134.—Illustration of velocity distribution for uncambered blade of conventional thickness at zero incidence angle. Data for 65–(0)10 blade of reference 39.

zero-camber thickness effect will appear only for blade-chord angles between 0° and 90°, since, as indicated by the highly simplified one-dimensional model of the blade passage flow in figure 135, the velocity distributions at these limit angles are symmetrical.

The effect of blade thickness blockage on impact-free-entry incidence angle for straight (uncambered) blades of constant chordwise thickness in incompressible two-dimensional flow is investigated in reference 34. The results of reference 34 are plotted in terms of the parameters used in this analysis in figure 136. It is reasonable to expect that similar trends of variations of zero-camber reference minimum-loss incidence angle will be obtained for compressor blade profiles.

On the basis of the preceding analysis, therefore, it is expected that, for low-speed-cascade flow, reference minimum-loss incidence angle will generally be positive at zero camber and decrease with increasing camber, depending on solidity and blade-chord angle. The available theory also indicates that the variation of reference incidence angle with camber at fixed solidity and chord angle might be essentially linear. If so, the variations could be expressed in terms of slope

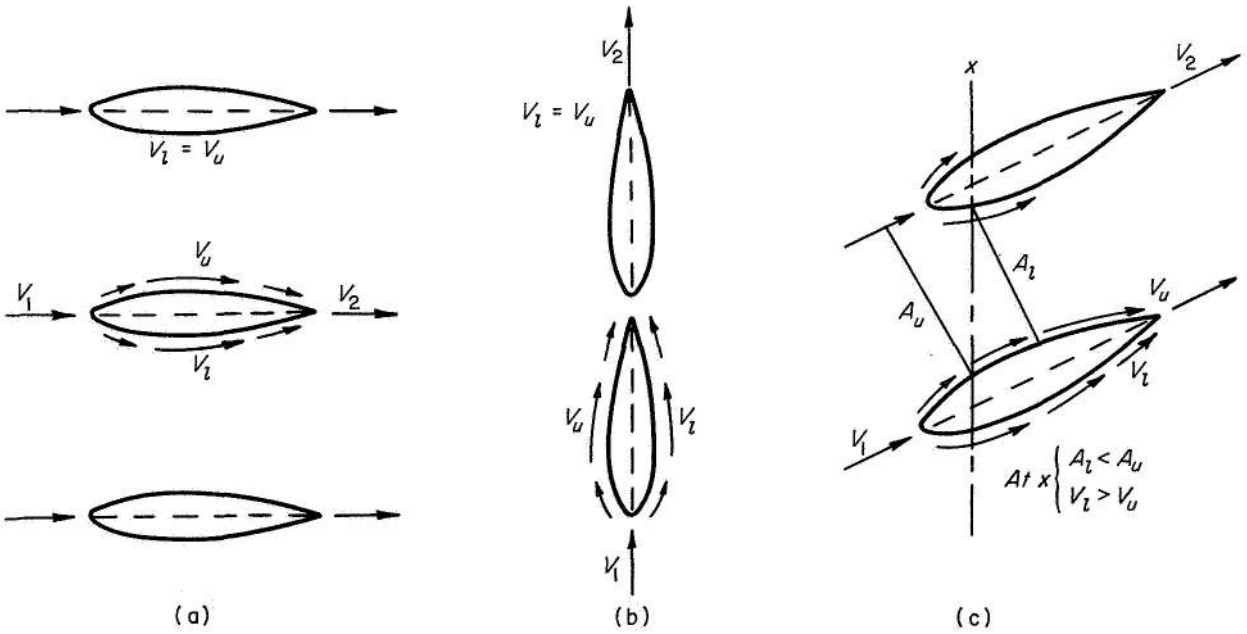

(a) $\gamma°=0°$. (b) $\gamma°=90°$. (c) $0°<\gamma°<90°$.

FIGURE 135.—Effect of blade thickness of surface velocity at zero incidence angle for uncambered airfoil section according to simplified one-dimensional model.

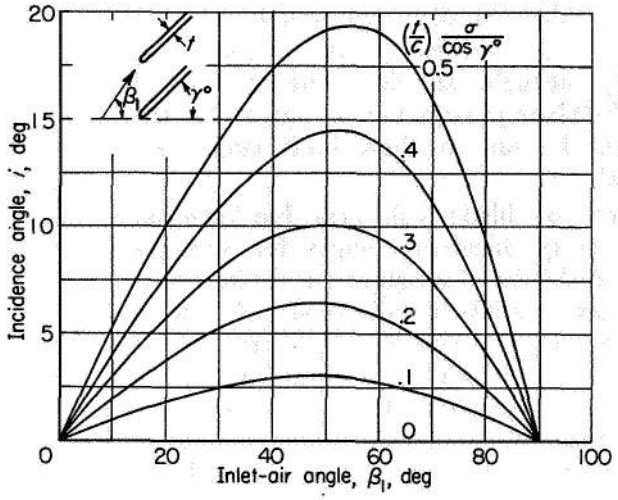

FIGURE 136.—Theoretical variation of "impact-free-entry" incidence angle for constant-thickness uncambered sections according to developments of reference 34.

and intercept values, where the intercept value represents the magnitude of the incidence angle for the uncambered section (function of blade thickness, solidity, and blade-chord angle). Reference minimum-loss incidence angle may also vary with inlet Mach number and possibly with Reynolds number.

DATA CORRELATIONS

Form of correlation.—Although preliminary theory indicates that blade-chord angle is the significant blade orientation parameter, it was necessary to establish the data correlations in terms of inlet-air angle, as mentioned previously. The observed cascade data were found to be represented satisfactorily by a linear variation of reference incidence angle with camber angle for fixed solidity and inlet-air angle. The variation of reference minimum-loss incidence angle can then be described in equation form as

$$i=i_o+n\varphi \tag{261}$$

where i_o is the incidence angle for zero camber, and n is the slope of the incidence-angle variation with camber $(i-i_o)/\varphi$.

Since the existence of a finite blade thickness is apparently the cause of the positive values of i_o, it is reasonable to assume that both the magnitude of the maximum thickness and the thickness distribution contribute to the effect. Therefore, since the 10-percent-thick 65-series blades of reference 39 are to be used as the basis for a generalized correlation of all conventional blade shapes, it is proposed that the zero-camber reference incidence angle be expressed in the form

$$i_o=(K_i)_{sh}(K_i)_t(i_o)_{10} \tag{262}$$

where $(i_o)_{10}$ represents the variation of zero-camber incidence angle for the 10-percent-thick 65-series thickness distribution, $(K_i)_t$ represents any correction necessary for maximum blade thicknesses other than 10 percent, and $(K_i)_{sh}$ represents any correction necessary for a blade shape with a thickness distribution different from that of the 65-series blades. (For a 10-percent-thick 65-series blade, $(K_i)_t=1$ and $(K_i)_{sh}=1$.)

The problem, therefore, is reduced to finding the values of n and i_o (through eq. (262)) as functions of the pertinent variables involved for the various blade profiles considered.

NACA 65-(A_{10})-series blades.—From the extensive low-speed-cascade data for the 65-(A_{10})-series blades (ref. 39), when expressed in terms of equivalent incidence and camber angles (figs. 125 and 126), plots of i_o and n can be deduced that adequately represent the minimum-loss-incidence-angle variations of the data. The deduced values of i_o and n as functions of solidity and inlet-air angle are given for these blades in figures 137 and 138. The subscript 10 in figure 137 indicates that the i_o values are for 10-percent maximum-thickness ratio. Values of intercept i_o and slope n were obtained by fitting a straight line to each data plot of reference incidence angle against camber angle for a fixed solidity and air inlet angle. The straight lines were selected so that both a satisfactory representation of the variation of the data points and a consistent variation of the resulting n and i_o values were obtained.

The deduced rule values and the observed data points compared in figure 139 indicate the effectiveness of the deduced representation. In several configurations, particularly for low cambers, the range of equivalent incidence angle covered in the tests was insufficient to permit an accurate determination of a minimum-loss value. Some of the scatter of the data may be due to the effects of local laminar separation in altering the range characteristics of the sections.

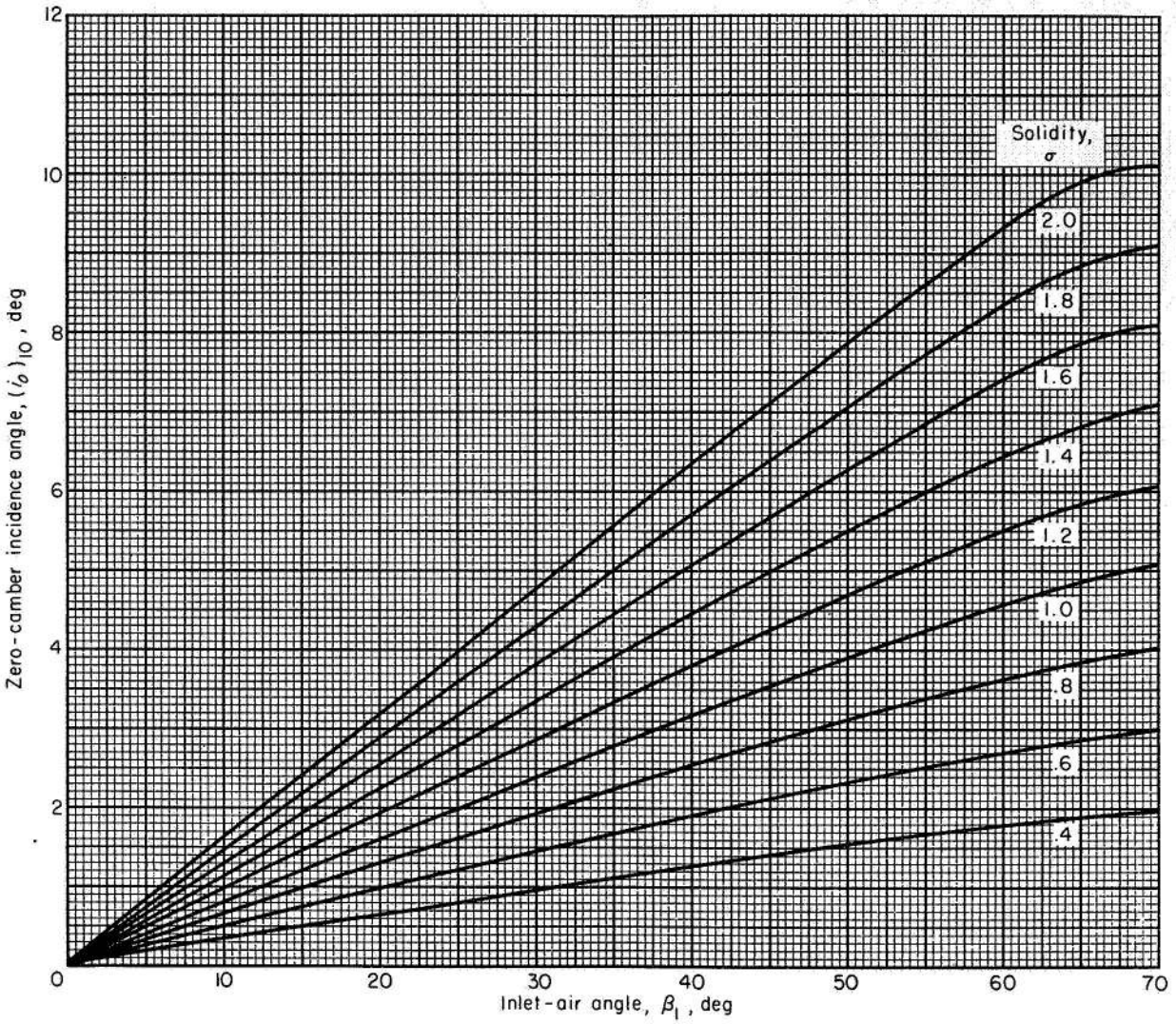

FIGURE 137.—Reference minimum-loss incidence angle for zero camber deduced from low-speed-cascade data of 10-percent-thick NACA 65-(A_{10})-series blades (ref. 39).

Although the cascade data in reference 39 include values of inlet-air angle from 30° to 70° and values of solidity from 0.5 to 1.5, the deduced variations in figures 137 and 138 are extrapolated to cover wider ranges of β_1 and σ. The extrapolation of i_o to zero at $\beta_1=0$ is obvious. According to theory (fig. 133), the value of the slope term does not vanish at $\beta_1=0$. In figure 138, therefore, an arbitrary fairing of the curves down to nonzero values of n was adopted as indicated. Actually, it is not particularly critical to determine the exact value of the slope term at $\beta_1=0$ necessary to locate the reference incidence angle precisely, since, for such cases (inlet guide vanes and turbine nozzles), a wide low-loss range of operation is usually obtained. The solidity extrapolations were attempted because of the uniform variations of the data with solidity. However, caution should be exercised in any further extrapolation of the deduced variations.

C-Series circular-arc blades.—The various thickness distributions used in combination with the circular-arc mean line have been designated C.1, C.2, C.3, and so forth (refs. 196 to 198). In general, the various C-series thickness distributions are fairly similar, having their maximum thickness located at between 30 and 40 percent of the chord length. The 65-series and two of

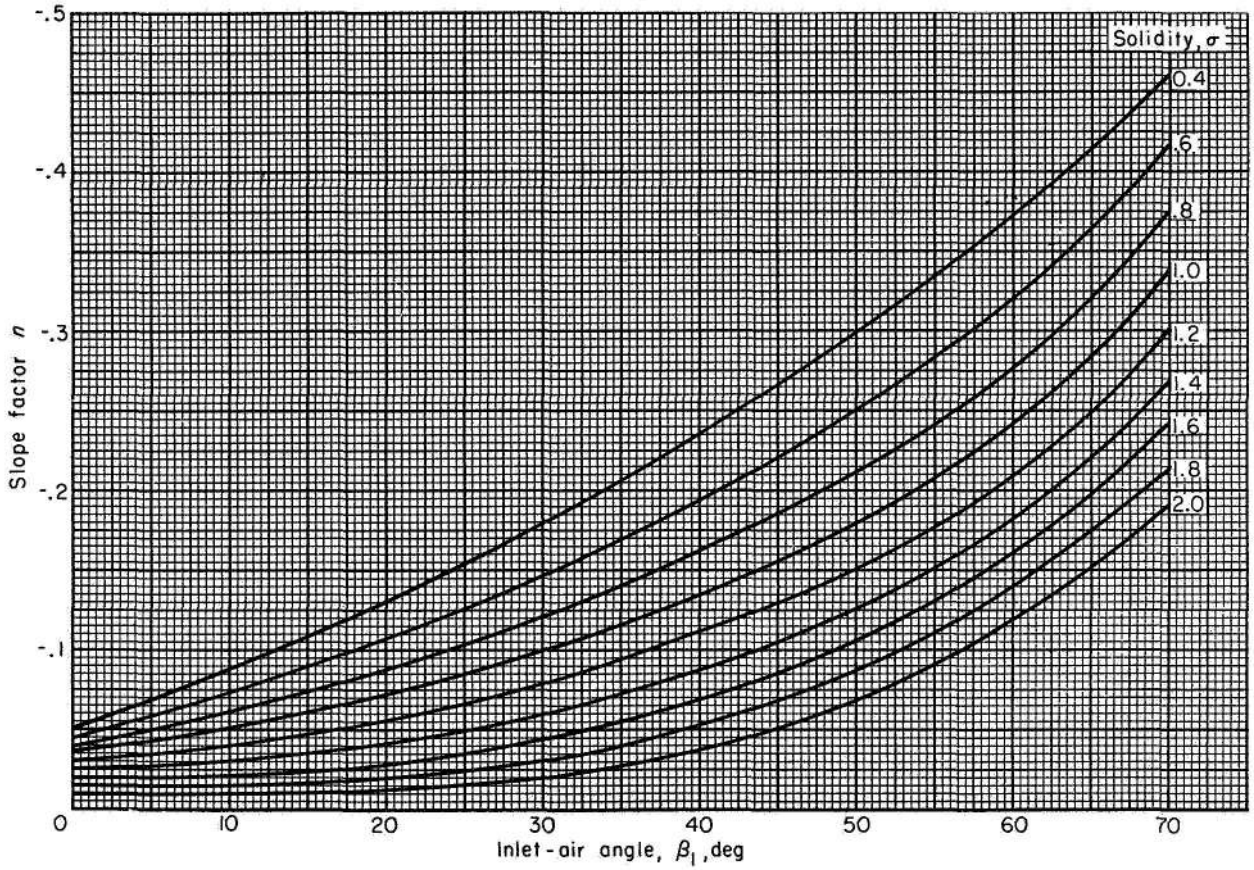

FIGURE 138.—Reference minimum-loss-incidence-angle slope factor deduced from low-speed-cascade data for NACA 65-(A_{10})-series blades as equivalent circular arcs.

the more popular C-series thickness distributions (C.1 and C.4) are compared on an exaggerated scale in figure 140. (The 65-series profile shown is usually thickened near the trailing edge in actual blade construction.)

In view of the somewhat greater thickness blockage in the forward portions of the C-series blades (fig. 140), it may be that the minimum-loss incidence angles for zero camber for the C-series blades are somewhat greater than those for the 65-series profiles; that is, $(K_i)_{sh}>1$. In the absence of any definitive cascade data, the value of $(K_i)_{sh}$ for the C-series profiles was arbitrarily taken to be 1.1. Observed minimum-loss incidence angles for an uncambered 10-percent-thick C.4 profile (obtained from ref. 192, pt. I) are compared in figure 141 with values predicted from the deduced $(i_o)_{10}$ values for the 65-series blade (fig. 137 and eq. (262)) with an assumed value of $(K_i)_{sh}=1.1$. (For 10-percent thickness, $(K_i)_t=1$.)

In view of the similarity between the 65-(A_{10})-series mean line and a true circular arc (fig. 125), the applicability of the slope values in figure 138 to the circular-arc mean line was investigated. For the recent cascade data obtained from tunnels having good boundary-layer control (refs. 167, (pt. I) and 199), a check calculation for the 10-percent-thick C.4 circular-arc blades using figures 137 and 138 with $(K_i)_{sh}=1.1$ revealed good results. For the three configurations in reference 199 tested at constant $\beta_1(\varphi=30°)$, the agreement between observed and predicted minimum-loss incidence angles was within 1°. For the one configuration in reference 167 (pt. I) tested at constant $\gamma°(\varphi=31°)$, the predicted value of minimum-loss incidence angle was 1.7° greater than the observed value. However, in view of the general 1° to 2° difference between fixed β_1 and fixed $\gamma°$ operation (fig. 132), such a discrepancy is to be expected. On the basis of these limited data, it appears that the low-speed minimum-loss incidence angles for the C-series circular-arc

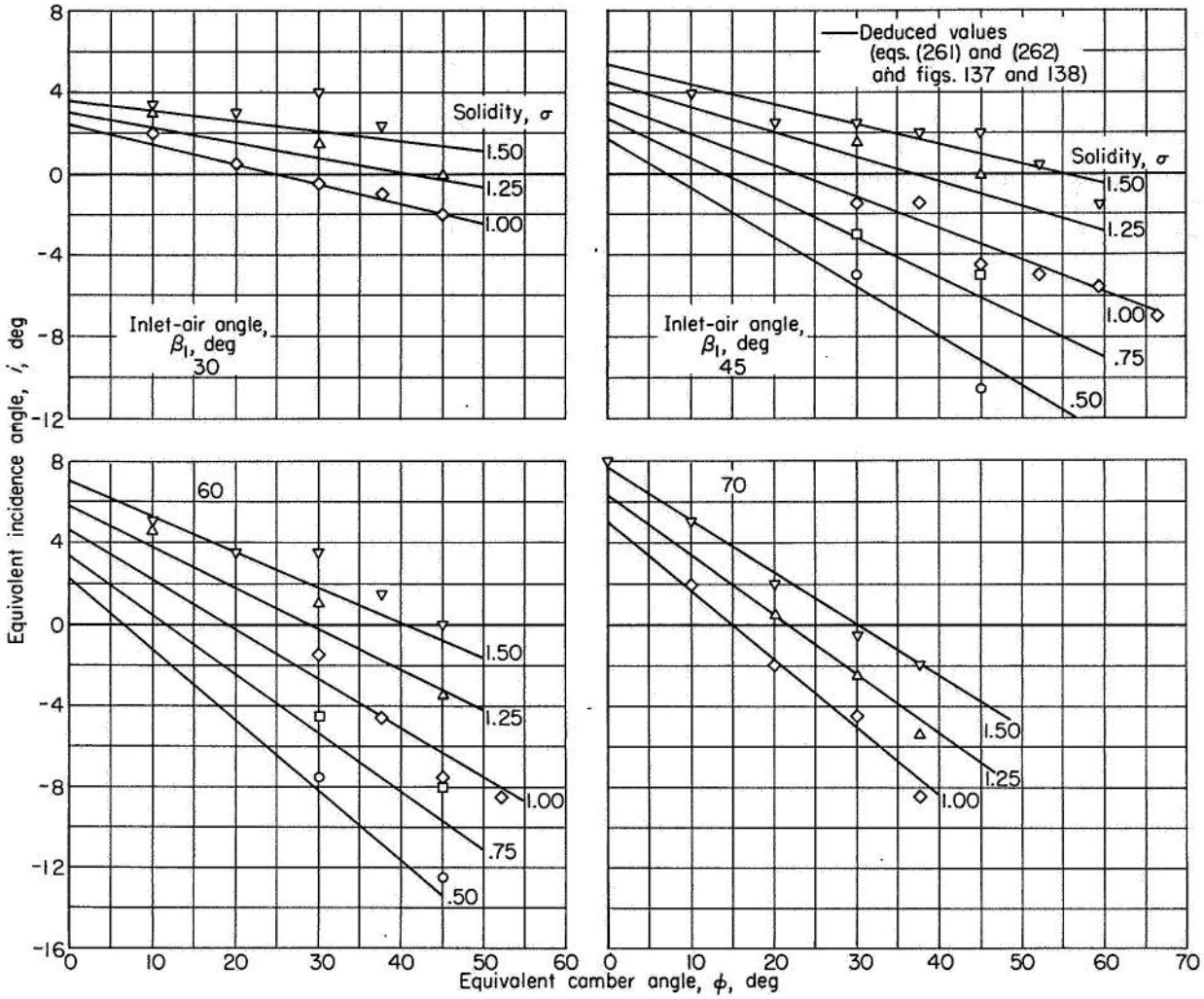

FIGURE 139.—Comparison of data values and deduced rule values of reference minimum-loss incidence angle for 65-(A_{10})10 blades as equivalent circular arc (ref. 39).

blade can be obtained from the i_o and n values of the 65-series blade with $(K_i)_{sh}=1.1$.

Double-circular-arc blades.—The double-circular-arc blade is composed of circular-arc upper and lower surfaces. The arc for each surface is drawn between the point of maximum thickness at midchord and the tangent to the circles of the leading- and trailing-edge radii. The chordwise thickness distribution for the double-circular-arc profile with 1-percent leading- and trailing-edge radius is shown in figure 140. Lack of cascade data again prevents an accurate determination of a reference-incidence-angle rule for the double circular arc. Since the double-circular-arc blade is thinner than the 65-series blade in the inlet region, the zero-camber incidence angles for the double-circular-arc blade should be somewhat different from those of the 65-series section, with perhaps $(K_i)_{sh}\leq 1$. It can also be assumed, as before, that the slope-term values of figure 138 are valid for the double-circular-arc blade. From an examination of the available cascade data for the double-circular-arc blade ($\varphi=25°$, $\sigma=1.333$, ref. 40; and $\varphi=40°$, $\sigma=1.064$, ref. 197), it appears that the use of figures 137 and 138 with a value of $(K_i)_{sh}=0.7$ in equations (261) and (262) results in a satisfactory comparison between predicted and observed values of reference incidence angle.

Other blades.—Similar procedures can be applied to establish reference-incidence-angle correlations for other blade shapes. Cascade data

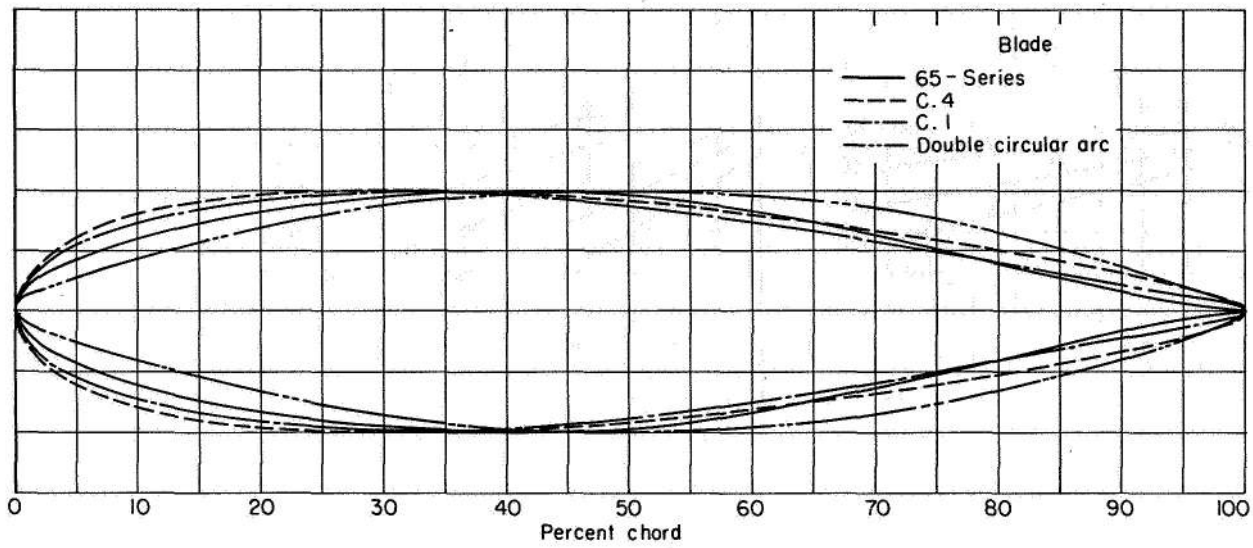

FIGURE 140.—Comparison of basic thickness distributions for conventional compressor blade sections.

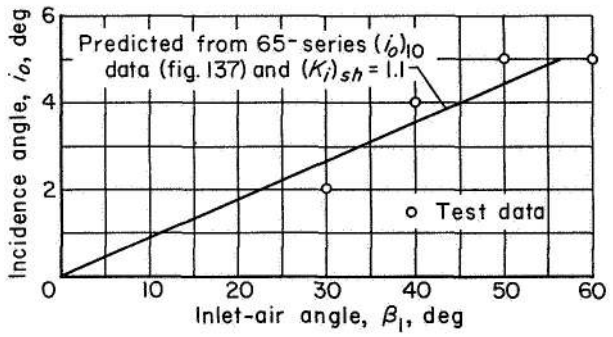

FIGURE 141.—Zero-camber minimum-loss incidence angle angle for 10-percent-thick C.4 profile. Solidity, 1.0 (ref. 192, pt. I).

are also available for the C-series parabolic-arc blades (refs. 40, 192, 200, and 201) and the NACA 65-(AI)-series blade (ref. 123); but, in view of the limited use of these forms in current practice, no attempt was made at this time to deduce corresponding incidence-angle rules for these blades.

Effect of blade maximum thickness.—As indicated previously, some correction (expressed here in terms of $(K_t)_t$, eq. (262)) of the base values of $(i_o)_{10}$ obtained from the 10-percent-thick 65-series blades in figure 137 should exist for other values of blade maximum-thickness ratio. According to the theory of the zero-camber effect, $(K_t)_t$ should be zero for zero thickness and increase as maximum blade thickness is increased, with a value of 1.0 for a thickness ratio of 0.10. Although the very limited low-speed data obtained from blades of variable thickness ratio (refs. 202 and 203) are not completely definitive, it was possible to establish a preliminary thickness-correction factor for reference zero-camber incidence angle as indicated in figure 142 for use in conjunction with equation (262).

Effect of inlet Mach number.—The previous correlations of reference minimum-loss incidence angle have all been based on low-speed-cascade data. It appears from limited high-speed data, however, that minimum-loss incidence angle will vary with increasing inlet Mach number for certain blade shapes.

The variations of minimum-loss incidence angle with inlet Mach number are plotted for several blade shapes in figures 143 and 144. The extension of the test data points to lower values of inlet Mach number could not generally be made because of reduced Reynolds numbers or insufficient points to establish the reference location at the lower Mach numbers. In some instances, however, it was possible to obtain low-speed values of incidence angle from other sources.

The blades of figure 143 show essentially no variation of minimum-loss incidence angle with inlet Mach number, at least up to a Mach number of about 0.8. The blades of figure 144, however, evidence a marked increase in incidence angle with Mach number. The difference in the variation of minimum-loss incidence angle with Mach number in figures 143 and 144 is associated with the

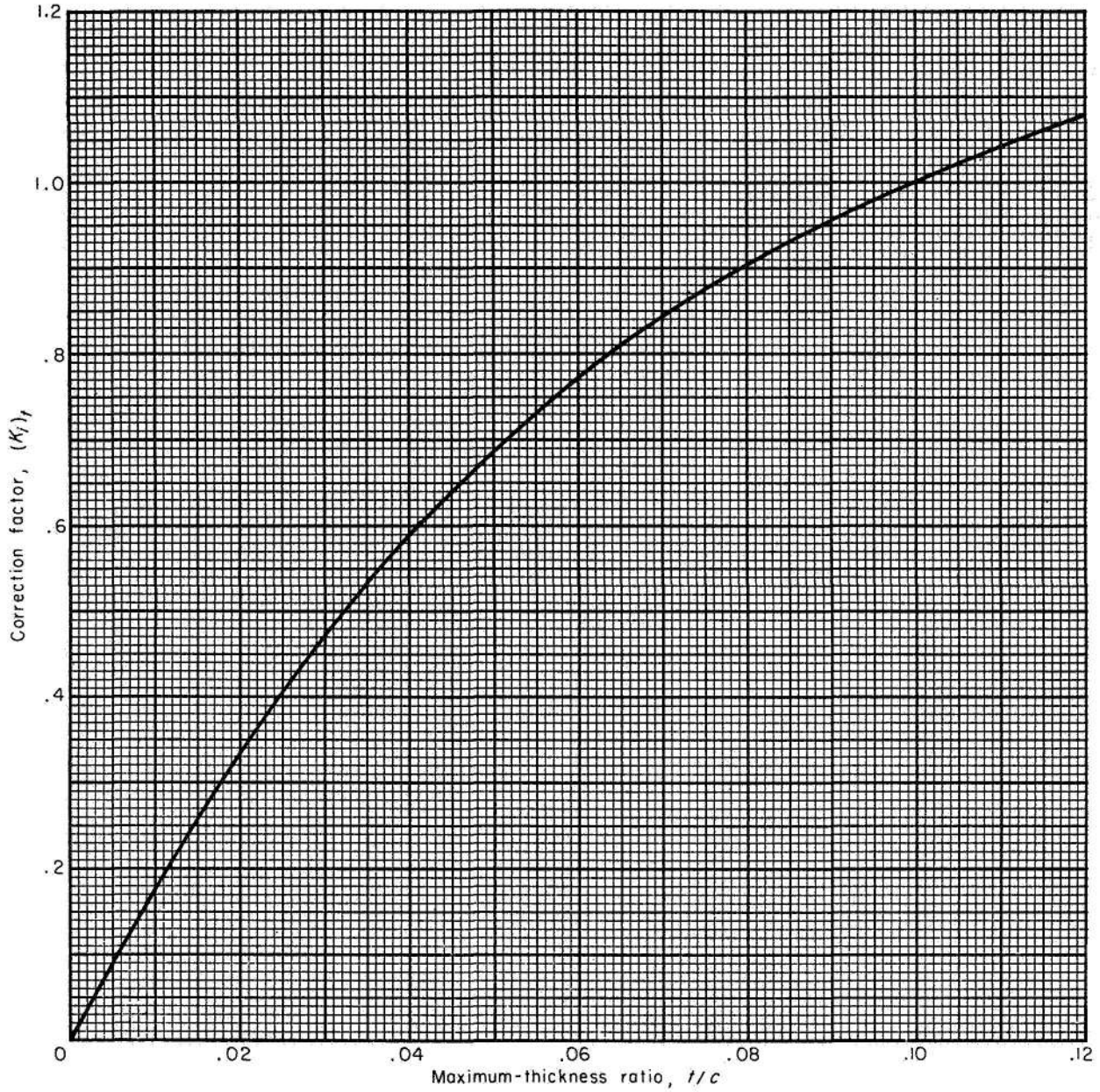

FIGURE 142.—Deduced blade maximum-thickness correction for zero-camber reference minimum-loss incidence angle (eq. (262)).

different way the general pattern of the loss variation changes with increasing Mach number for the two types of blades. For the thick-nose blades, as illustrated in figures 130 (a) and (b), the loss coefficient increases with Mach number at both the high and low incidence angles, thus tending to maintain the same point of minimum loss. For the sharp-nose blade, as illustrated by figures 130 (c) and (d), the increase in loss occurs primarily on the low-incidence-angle side; and a positive shifting of the minimum-loss incidence angle results. Data for other thick-nose sections in reference 201 show the rise in loss to occur at both ends of the curve, but plots of reference incidence angle against Mach number could not validly be

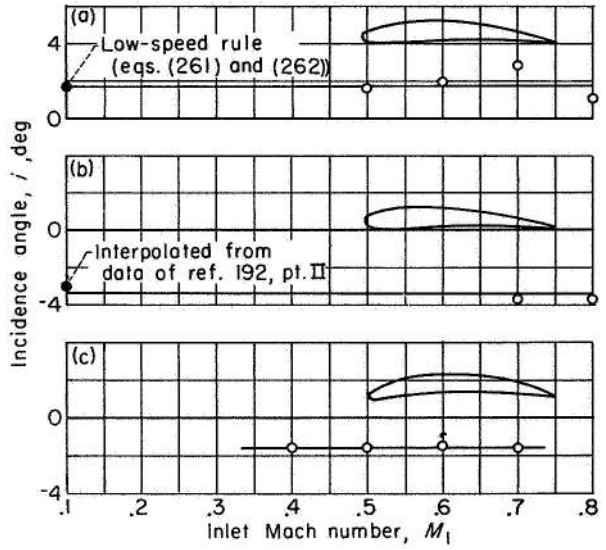

(a) C.4 Circular-arc blade. Camber angle, 25°; solidity 1.333; blade-chord angle, 42.5° (ref. 40).
(b) C.4 Parabolic-arc blade. Camber angle, 25°; solidity, 1.333; blade-chord angle, 37.5°; maximum camber at 40-percent chord (ref. 40).
(c) C.7 Parabolic-arc blade. Camber angle, 40°; solidity, 1.0; blade-chord angle, 24.6°; maximum camber at 45-percent chord (ref. 216).

FIGURE 143.—Variation of reference minimum-loss incidence angle with inlet Mach number for thick-nose sections. Maximum-thickness ratio, 0.10.

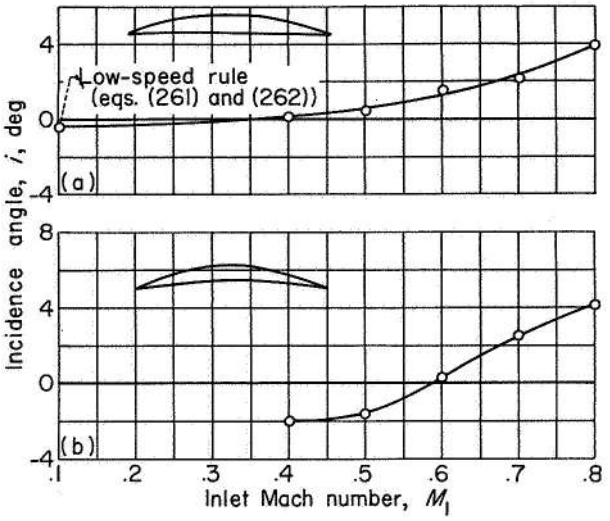

(a) Double-circular-arc blade. Camber angle, 25°; maximum-thickness ratio, 0.105; solidity, 1.333; blade-chord angle, 42.5° (ref. 40).
(b) Blade section of reference 205. Camber angle, 27.5°; maximum-thickness ratio, 0.08; solidity, 1.15; blade-chord angle, 30°; maximum thickness and camber at 50-percent chord.

FIGURE 144.—Variation of reference minimum-loss incidence angle with inlet Mach number for sharp-nose sections.

made for these blades because of evidence of strong local laminar-separation effects.

Since the most obvious difference between the blades in figures 143 and 144 is the construction of the leading-edge region, the data suggest that blades with thick-nose inlet regions tend to show, for the range of inlet Mach number covered, essentially no Mach number effect on minimum-loss incidence angle, while blades with sharp leading edges will have a significant Mach number effect. The available data, however, are too limited to confirm this observation conclusively at this time. Furthermore, for the blades that do show a Mach number effect, the magnitude of the variation of reference incidence angle with Mach number is not currently predictable.

SUMMARY

The analysis of blade-section reference minimum-loss incidence angle shows that the variation of the reference incidence angle with cascade geometry at low speed can be established satisfactorily in terms of an intercept value i_o and a slope value n as given by equation (261). Deduced values of i_o and n were obtained as a function of β_1 and σ from the data for the 10-percent-thick 65-(A_{10})-series blades of reference 39 as equivalent circular-arc sections (figs. 137 and 138). It was then shown that, as a first approach, the deduced values of $(i_o)_{10}$ and n in figures 137 and 138 could also be used to predict the reference incidence angles of the C-series and double-circular-arc blades by means of a correction $(K_i)_{sh}$ to the $(i_o)_{10}$ values of figure 137 (eq. (262)).

The procedure involved in estimating the low-speed reference minimum-loss incidence angle of a blade section is as follows: From known values of β_1 and σ, $(i_o)_{10}$ and n are selected from figures 137 and 138. The value of $(K_i)_t$ for the blade maximum-thickness ratio is obtained from figure 142, and the appropriate value of $(K_i)_{sh}$ is selected for the type of thickness distribution. For NACA 65-series blades, $(K_i)_{sh}=1.0$; and it is proposed that $(K_i)_{sh}$ be taken as 1.1 for the C-series circular-arc blade and as 0.7 for the double-circular-arc blade. The value of i_o is then computed from equation (262); and finally i is determined from

the blade camber angle according to equation (261).

It should be noted that the values of $(K_i)_{sh}$ given for the circular-arc blades are rather tenuous values obtained from very limited data. The use of the proposed values is not critical for good accuracy; the values were included primarily for completeness as a reflection of the anticipated differences in the blade thickness blockage effects. Further experimental data will be necessary to establish the significance of such a correction. Also, a marked increase in reference minimum-loss incidence angle with Mach number is to be expected for sharp-nose blade sections. The magnitude of the Mach number correction for these blades is currently unpredictable.

LOSS ANALYSIS

With the location of the low-speed reference minimum-loss incidence angle established for several conventional blade sections, the magnitude of the losses occurring at this reference position (fig. 127) will now be investigated. Accordingly, the nature of the loss phenomena and the various factors influencing the magnitude of the loss over a range of blade configurations and flow conditions are first analyzed. The available experimental loss data are then examined to establish fundamental loss correlations in terms indicated by the analysis.

PRELIMINARY ANALYSIS

Two-dimensional-cascade losses arise primarily from the growth of boundary layer on the suction and pressure surfaces of the blades. These surface boundary layers come together at the blade trailing edge, where they combine to form the blade wake, as shown in figure 145. As a result of the formation of the surface boundary layers, a local defect in total pressure is created, and a certain mass-averaged loss in total pressure is determined in the wake of the section. The loss in total pressure is measured in terms of the total-pressure-loss coefficient $\bar{\omega}$, defined generally as the ratio of the mass-averaged loss in total pressure $\overline{\Delta P}$ across the blade row from inlet to outlet stations to some reference free-stream dynamic pressure $(P_0-p_0)_{ref}$, or

$$\bar{\omega}_{ref}=\frac{\overline{\Delta P}}{(P_0-p_0)_{ref}} \tag{263}$$

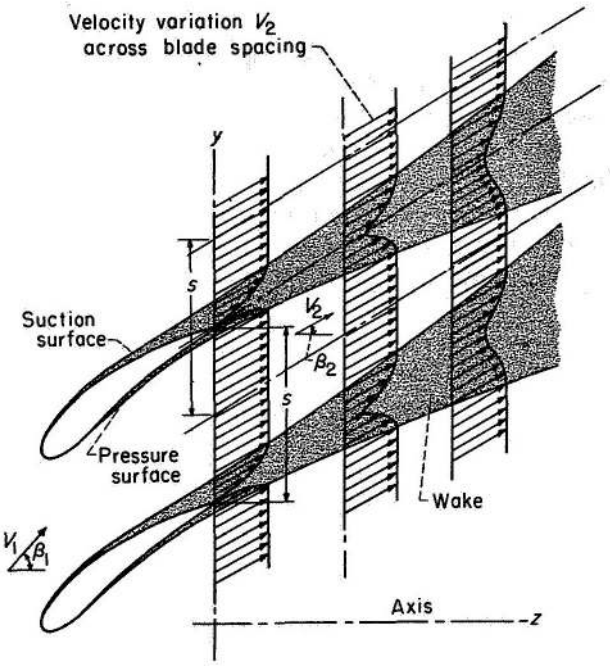

FIGURE 145.—Schematic representation of development of surface boundary layers and wake in flow about cascade blade sections.

For incompressible flow, P_0-p_0 is equal to the conventional free-stream dynamic pressure $\rho_0 V_0^2/2$. The total-pressure-loss coefficient is usually determined from consideration of the total-pressure variation across a blade spacing s (fig. 145).

A theoretical analysis of incompressible two-dimensional-cascade losses in reference 156 shows that the total-pressure-loss coefficient at the cascade-outlet measuring station (where the static pressure is essentially uniform across the blade spacing) is given by

$$\bar{\omega}_1=2\left(\frac{\theta^*}{c}\right)_2\frac{\sigma}{\cos\beta_2}\left(\frac{\cos\beta_1}{\cos\beta_2}\right)^2\left\{\frac{\frac{2H_2}{3H_2-1}}{\left[1-\left(\frac{\theta^*}{c}\right)_2\frac{\sigma H_2}{\cos\beta_2}\right]^3}\right\} \tag{264}$$

where $\bar{\omega}_1$ is the loss coefficient based on inlet dynamic head, θ^*/c is the ratio of wake momentum thickness to blade-chord length, σ is cascade solidity, β_2 is the air outlet angle, and H_2 is the wake form factor (displacement thickness divided by momentum thickness). The wake characteristics in equation (264) are expressed in terms of

conventional thickness in a plane normal to the wake (i.e., normal to the outlet flow) at the measuring station. Definitions of wake characteristics and variations in velocity and pressure assumed by the analysis are given in reference 156. The analysis further indicates that the collection of terms within the braces is essentially secondary (since H_2 is generally $\leq$ about 1.2 at the measuring station), with a magnitude of nearly 1 for conventional unstalled configurations. The principal determinants of the loss in total pressure at the cascade measuring station are, therefore, the cascade geometry factors of solidity, air outlet and air inlet angles, and the aerodynamic factor of wake momentum-thickness ratio.

Since the wake is formed from a coalescing of the pressure- and suction-surface boundary layers, the wake momentum thickness naturally depends on the development of the blade surface boundary layers and also on the magnitude of the blade trailing-edge thickness. The results of references 156, 202, and 204 indicate, however, that the contribution of conventional blade trailing-edge thickness to the total loss is not generally large for compressor sections; the preliminary factor in the wake development is the blade surface boundary-layer growth. In general, it is known (ch. V, e.g.) that the boundary-layer growth on the surfaces of the blade is a function primarily of the following factors: (1) the surface velocity gradients (in both subsonic and supersonic flow), (2) the blade-chord Reynolds number, and (3) the free-stream turbulence level.

Experience has shown that blade surface velocity distributions that result in large amounts of diffusion in velocity tend to produce relatively thick blade boundry layers. The magnitude of the velocity diffusion in low-speed flow generally depends on the geometry of the blade section and its incidence angle. As Mach number is increased, however, compressibility exerts a further influence on the velocity diffusion of a given cascade geometry and orientation. If local supersonic velocities develop at high inlet Mach numbers, the velocity diffusion is altered by the formation of shock waves and the interaction of these shock waves with the blade surface boundary layers. The losses associated with local supersonic flow in a cascade are generally greater than for subsonic flow in the same cascade. The increases in loss are frequently referred to as shock losses.

Cascade-inlet Mach number also influences the magnitude of the subsonic diffusion for a fixed cascade. This Mach number effect is the conventional effect of compressibility on the blade velocity distributions in subsonic flow. Compressibility causes the maximum local velocity on the blade surface to increase at a faster rate than the inlet and outlet velocities. Accordingly, the magnitude of the surface diffusion from maximum velocity to outlet velocity becomes greater as inlet Mach number is increased. A further secondary influence of Mach number on losses is obtained because of an increase in losses associated with the eventual mixing of the wake with the surrounding free-stream flow (ref. 37).

On the basis of the foregoing considerations, therefore, it is expected that the principal factors upon which to base empirical cascade-wake-thickness correlations should be velocity diffusion, inlet Mach number, blade-chord Reynolds number, and, if possible, turbulence level.

DATA CORRELATIONS

Velocity diffusion based on local velocities.— Recently, several investigations have been reported on the establishment of simplified diffusion parameters and the correlation of cascade losses in terms of these parameters (refs. 9, 38, and 156). The general hypothesis of these diffusion correlations states that the wake thickness, and consequently the magnitude of the loss in total pressure, is proportional to the diffusion in velocity on the suction surface of the blade in the region of the minimum loss. This hypothesis is based on the consideration that the boundary layer on the suction surface of conventional compressor blade sections contributes the major share of the wake in these regions, and therefore the suction-surface velocity distribution becomes the governing factor in the determination of the loss. It was further established in these correlations that, for conventional velocity distributions, the diffusion in velocity can be expressed significantly as a parameter involving the difference between some function of the measured maximum suction-surface velocity V_{max} and the outlet velocity V_2.

Reference 38 presents an analysis of blade-loading limits for the 65-(A_{10})10 blade section in terms of drag coefficient and a diffusion parameter given for incompressible flow by $(V_{max}^2-V_2^2)/V_{max}^2$.

Results of an unpublished analysis of cascade losses in terms of the momentum thickness of the blade wake (as suggested in ref. 156) indicate that a local diffusion parameter in the form given previously or in the form $(V_{max}-V_2)/V_{max}$ can satisfactorily correlate experimental cascade loss data.[2] The term "local diffusion parameter" is used to indicate that a knowledge of the maximum local surface velocity is required. The correlation obtained between calculated wake momentum-thickness ratio θ^*/c and local diffusion factor given by

$$D_{loc}=\frac{V_{max}-V_2}{V_{max}} \tag{265}$$

obtained for the NACA 65-(A_{10})-series cascade sections of reference 39 at reference incidence angle is shown in figure 146. Values of wake momentum-thickness ratio for these data were computed from the reported wake coefficient values according to methods similar to those discussed in reference 156. Unfortunately, blade surface velocity-distribution data are not available for the determination of the diffusion factor for other conventional blade shapes.

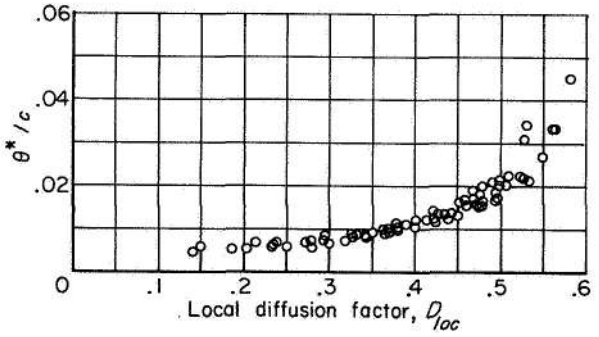

FIGURE 146.—Variation of computed wake momentum-thickness ratio with local diffusion factor at reference incidence angle for low-speed-cascade data of NACA 65-(A_{10})10 blades (ref. 39).

The correlation of figure 146 indicates the general validity of the basic diffusion hypothesis. At high values of diffusion (greater than about 0.5), a separation of the suction-surface boundary layer is suggested by the rapid rise in the momentum thickness. The indicated nonzero value of momentum thickness at zero diffusion represents the basic friction loss (surface shear stress) of the flow and also, to a smaller extent, the effect of the finite trailing-edge thickness. The correlation of figure 146 further indicates that wake momentum-thickness ratio at reference incidence angle can be estimated from the computed local diffusion factor for a wide range of solidities, cambers, and inlet-air angles. The loss relations of equation (264) and reference 156 can then be used to compute the resulting loss in the total pressure.

Velocity diffusion based on over-all velocities.—In order to include the cases of blade shapes for which velocity-distribution data are not available, a diffusion parameter has been established in reference 9 that does not require a specific knowledge of the peak local suction-surface velocity. Although originally derived for use in compressor design and analysis, the diffusion factor of reference 9 can also be applied in the analysis of cascade losses. The diffusion factor of reference 9 attempts, through several simplifying approximations, to express the local diffusion on the blade suction surface in terms of over-all (inlet or outlet) velocities or angles, quantities that are readily determined. The basis for the development of the over-all diffusion factor is presented in detail in reference 9 and is indicated briefly in figure 147. The diffusion factor is given by

$$D=\left(1-\frac{V_2}{V_1}\right)+\frac{\Delta V_\theta}{2\sigma V_1} \tag{54}$$

which, for incompressible two-dimensional-cascade flow, becomes

$$D=\left(1-\frac{\cos\beta_1}{\cos\beta_2}\right)+\frac{\cos\beta_1}{2\sigma}(\tan\beta_1-\tan\beta_2) \tag{266}$$

As in the case of the local diffusion factor, the diffusion factor of equation (266) is restricted to the region of minimum loss.

Cascade total-pressure losses at reference minimum-loss incidence angle are presented in reference 9 as a function of diffusion factor for the blades of reference 39. In a further unpublished analysis, a composite plot of the variation of computed wake momentum-thickness ratio with D at reference minimum-loss incidence angle was obtained from the available systematic cascade data (refs. 39 and 192) as shown in figure 148.[2] Blade maximum thickness was 10 percent in all

[2] A later analysis of cascade total-pressure losses is given in Analysis of Experimental Low-Speed Loss and Stall Characteristics of Two-Dimensional Compressor Blade Cascades by Seymour Liebein, NACA RM E57A28, 1957.

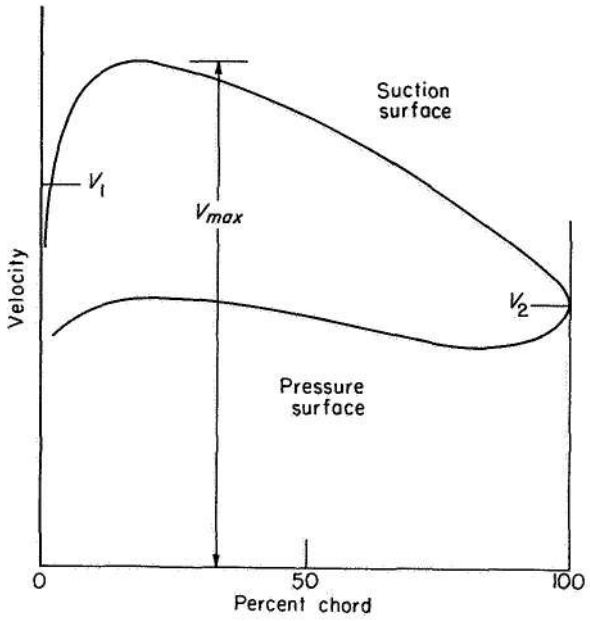

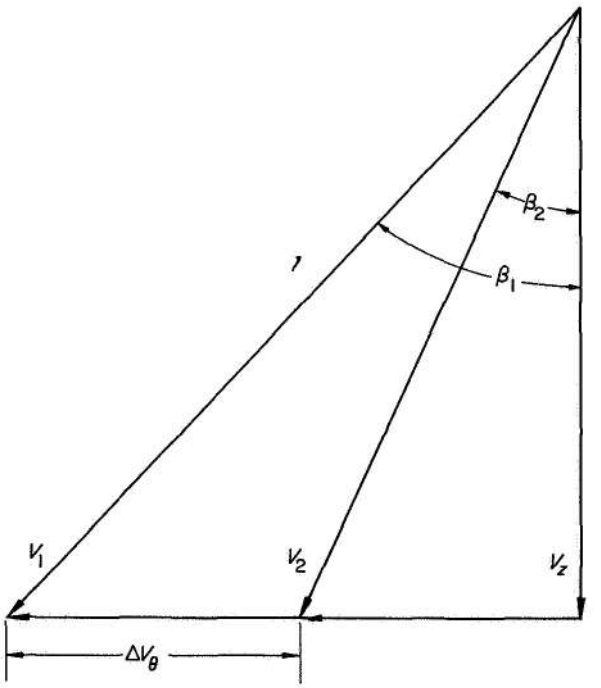

FIGURE 147.—Basis of development of diffusion factor for cascade flow from reference 9. $D \approx \frac{V_{max}-V_2}{V_{av}} \approx \frac{V_{max}-V_2}{V_1}$; $V_{max} \approx V_1 + f\left(\frac{\Delta V\theta}{\sigma}\right)$; thus, equations (54) and (266).

cases. A separation of the suction-surface boundary layer at high blade loading is indicated

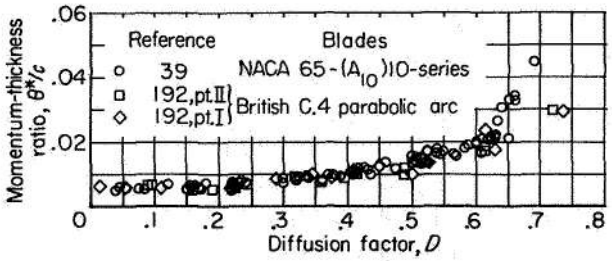

FIGURE 148.—Variation of computed wake momentum-thickness ratio with overall diffusion factor at reference incidence angle for low-speed systematic cascade data of references 39 and 192. Blade maximum-thickness ratio, 0.10; Reynolds number, $\approx 2.5 \times 10^5$.

by the increased rise in the wake momentum thickness for values of diffusion factor greater than about 0.6.

For situations in which the determination of a wake momentum-thickness ratio cannot be made, a significant loss analysis may be obtained if a simplified total-pressure-loss parameter is used that closely approximates the wake thickness. Since the terms within the braces of equation (264) are generally secondary factors, a loss parameter of the form $\bar{\omega}_1 \frac{\cos \beta_2}{2\sigma}\left(\frac{\cos \beta_2}{\cos \beta_1}\right)^2$ should constitute a more fundamental expression of the basic loss across a blade element than the loss coefficient alone. The effectiveness of this substitute loss parameter in correlating two-dimensional-cascade losses is illustrated in figure 149(a) for all the data for the NACA 65-(A_{10})-series blades of reference 39. (Total-pressure-loss coefficients were computed for the data from relations given in ref. 9.) A generalized correlation can also be obtained in terms of $\bar{\omega}_1 \frac{\cos \beta_2}{2\sigma}$, as shown in figure 149(b), but its effectiveness as a separation indicator does not appear to be as good. Such generalized loss parameters are most effective if the wake form does not vary appreciably among the various data considered.

Effect of blade maximum thickness.—Since an increase in blade maximum-thickness ratio increases the magnitude of the surface velocities (and therefore the diffusion), higher values of wake momentum-thickness ratio would be expected for thicker blades. From an analysis of limited available data on varying blade maximum-thickness ratio (refs. 202 and 203), it appears that the effect of blade thickness on wake momentum-thickness ratio is not large for conventional

cascade configurations. For example, for an increase in blade maximum-thickness ratio from 0.05 to 0.10, an increase in θ^*/c of about 0.003 at D of about 0.55 and an increase of about 0.002 at D of about 0.35 are indicated. The greater increase in wake θ^*/c at the higher diffusion level is understandable, since the rate of change of θ^*/c with D_{loc} increases with increasing diffusion (see fig. 146).

If blade surface velocity distributions can be determined, then the thickness effect will automatically be included in the evaluation of the resulting local diffusion factor. When an overall diffusion factor such as equation (54) is used, variations in blade thickness are not reflected in the corresponding loss prediction. However, in view of the small observed effect and the scatter of the original θ^*/c against D correlation of figure 148, it is believed that a thickness correction is unwarranted for conventional thickness ranges. However, the analysis does indicate that, for high diffusion and high solidity levels, it may be advisable to maintain blade thickness as small as practicable in order to obtain the lowest loss at the reference condition.

Thus, the plots of figures 146, 148, and 149 show that, when diffusion factor and wake momentum-thickness ratio (or total-pressure-loss parameter) are used as the basic blade-loading and loss parameters, respectively, a generalized correlation of two-dimensional-cascade loss data is obtained. Although several assumptions and restrictions are involved in the use and calculation of these parameters, the basic diffusion approach constitutes a useful tool in cascade loss analysis. In particular, the diffusion analysis should be investigated over the complete range of incidence angle in an effort to determine generalized off-design loss information.

Effect of Reynolds number and turbulence.—The effect of blade-chord Reynolds number and turbulence level on the measured losses of cascade sections is discussed in the section on Data Selection, in chapter V, and in references 39, 167 (pt. I), and 183. In all cases, the data reveal an increasing trend of loss coefficient with decreasing Reynolds number and turbulence. Examples of the variation of the total-pressure-loss coefficient with incidence angle for conventional compressor blade sections at two different values of Reynolds number are illustrated in figure

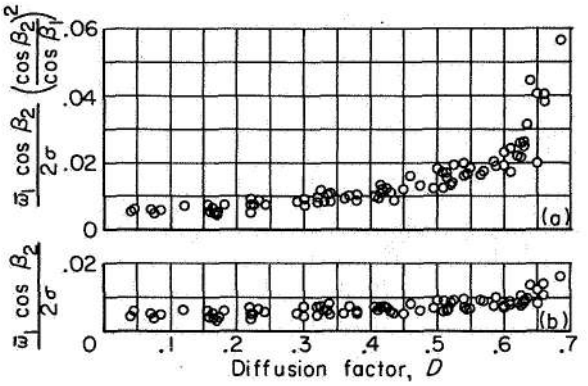

(a) Based on $\bar{\omega}_1 \left(\frac{\cos \beta_2}{\cos \beta_1}\right)^2$.

(b) Based on $\bar{\omega}_1$.

FIGURE 149.—Variation of loss parameter with diffusion factor at reference minimum-loss incidence angle computed from low-speed-cascade data of NACA 65-(A_{10})10 cascade blades (ref. 39).

150. Loss variations with Reynolds number over a range of incidence angles for a given blade shape are shown in figure 151. A composite plot of the variation of total-pressure-loss coefficient

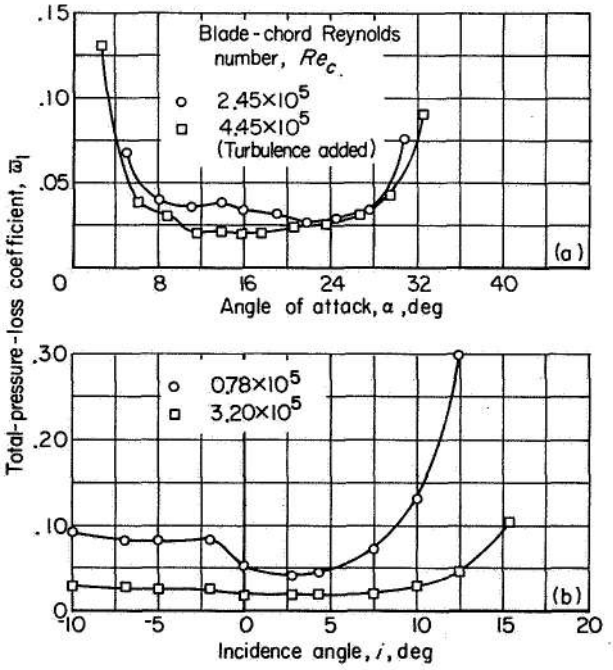

(a) 65-Series blade 65-(12)10. Solidity, 1.5; inlet-air angle, 45° (ref. 39).

(b) Circular-arc blade 10C4/25C50. Solidity, 1.333; blade-chord angle, 42.5° (ref. 40).

FIGURE 150.—Effect of Reynolds number on variation of loss with incidence angle.

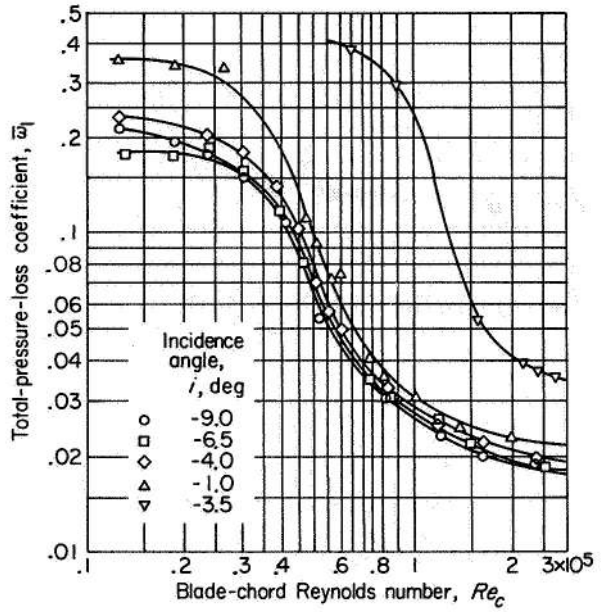

FIGURE 151.—Variation of total-pressure-loss coefficient with blade-chord Reynolds number for parabolic-arc blade 10C4/40 P40. Inlet-air angle, 28° to 40°; solidity, 1.333 (ref. 183).

at minimum loss with blade-chord Reynolds number for a large number of blade shapes is shown in figure 152. Identification data for the various blades included in the figure are given in the references. For the blades whose loss data are reported in terms of drag coefficient, conversion to total-pressure-loss coefficient was accomplished according to the cascade relations presented in reference 9. The effect of change in tunnel turbulence level through the introduction of screens is indicated for some of the blades.

It is apparent from the curves in figure 152 that it is currently impossible to establish any one value of limiting Reynolds number that will hold for all blade shapes. (The term limiting Reynolds number refers to the value of Reynolds number at which a large rise in loss is obtained.) On the basis of the available cascade data presented in figure 152, however, it appears that serious trouble in the minimum-loss region may be encountered at Reynolds numbers below about 2.5×10^5. Carter in reference 190 places the limiting blade-chord Reynolds number based on outlet velocity at 1.5 to 2.0×10^5. Considering that outlet Reynolds number is less than inlet Reynolds number for decelerating cascades, this quoted value is in effective agreement with the value of limiting Reynolds number deduced herein.

The desirability of conducting cascade investigations in the essentially flat range of the curve of loss coefficient against Reynolds number in order to enhance the correlation of data from various tunnels, as well as from the various configurations of a given tunnel, is indicated. Cascade operation in the flat range of Reynolds number may also yield a more significant comparison between observed and theoretically computed loss. Reynolds number and turbulence level should always be defined in cascade investigations. Furthermore, the development of some effective Reynolds number (ch. V) that attempts to combine the effects of both blade-chord Reynolds number and turbulence should be considered for use as the independent variable.

Effect of inlet Mach number.—In the previous correlations, attention was centered on the various factors affecting the loss of cascade blades for

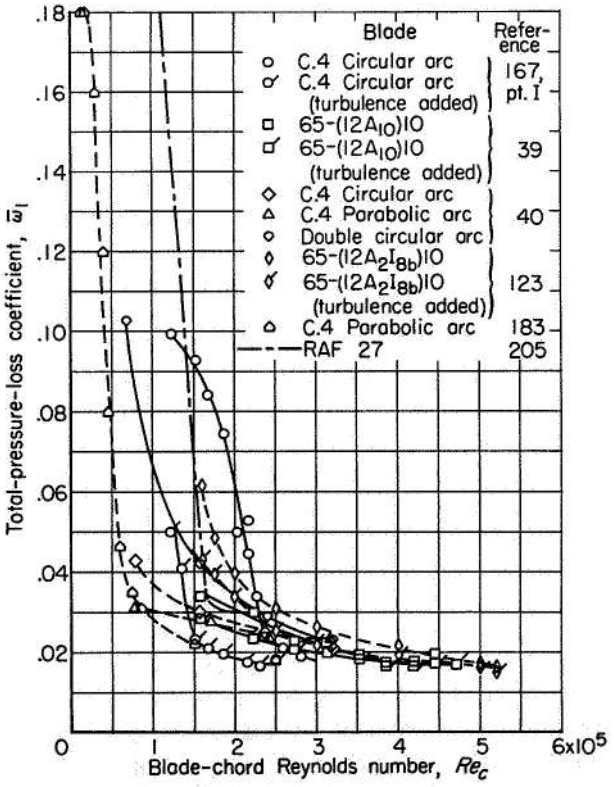

FIGURE 152.—Composite plot of loss coefficient against blade-chord Reynolds number in region of minimum loss for two-dimensional-cascade blade sections at low speed.

essentially incompressible or low Mach number flow. Tests of cascade sections at higher Mach number levels have been relatively few, primarily because of the large power requirements and operational difficulties of high-velocity tunnels. As a consequence, it has not been possible to establish any empirical correlations that will permit the estimation of Mach number effects for conventional blade sections. The limited available data indicate, however, that a marked rise in loss is eventually obtained as Mach number is increased.

A typical example of the variation of total-pressure-loss coefficient with inlet Mach number for a conventional cascade section at fixed incidence angle in the region of minimum loss is presented in figure 153(a). The inlet Mach number at which the sharp rise in loss occurs is referred to as the limiting Mach number. The variation of the wake profile downstream of the blade as Mach number is increased is shown in figure 153(b) to illustrate the general deterioration of the suction-surface flow. The flow deterioration is the result of a separation of the suction-surface boundary layer induced by shock-wave and boundary-layer interactions.

In view of the complex nature of the shock-wave development and its interaction effects, the estimation of the variation of minimum total-pressure loss with inlet Mach number for a given blade is currently impossible. At the moment, this pursuit must be primarily an experimental one. Schlieren photographs showing the formation of shocks in a cascade are presented in references 41, 205, and 206, and detailed discussions of shock formations and high-speed performance of two-dimensional-cascade sections are treated in references 41, 205, and 207 to 209. Cascade experience (refs. 40 and 205) and theory (refs. 41, 88, and 209) indicate that a location of the point of maximum thickness at about the 50-percent-chord position and a thinning of the blade leading and trailing edges are favorable for good high Mach number performance. The avoidance of a throat area within the blade passage is also indicated in order to minimize the effects of flow choking. Discussions of the choking problem are presented in references 203 and 208, and blade throat areas are given for several blade shapes in references 123 and 210 to 212. The effects of

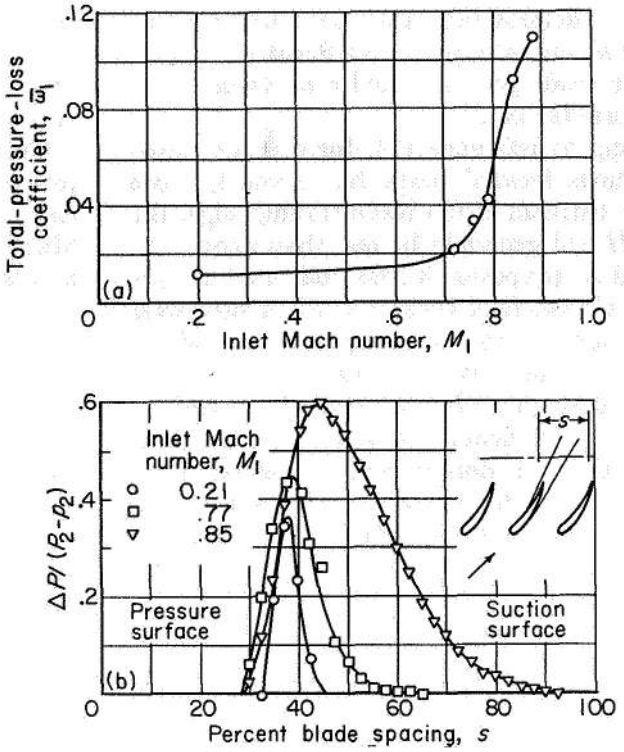

(a) Total-pressure-loss coefficient.
(b) Blade wake.

FIGURE 153.—Variation of cascade blade loss with inlet Mach number for NACA 65–($12A_{10}$)10 blade in region of minimum loss (ref. 122).

camber distribution on high Mach number performance are discussed extensively in the literature (refs. 123, 200, and 201). Results indicate that, for the range of blade shapes and Mach numbers normally covered, camber distribution does not have a large effect on maximum Mach number performance as obtained in the two-dimensional cascade.

SUMMARY

From the foregoing correlations and considerations, the low-speed loss in total pressure of conventional two-dimensional-cascade sections can readily be estimated. If blade surface velocity distributions are available, the suction-surface local diffusion factor D_{loc} is determined according to equation (265) and a value of θ^*/c is then selected from figure 146. In the absence of blade surface velocity data, the diffusion factor D is computed from over-all conditions by means of equation (54) and θ^*/c is selected from figure 148.

With θ^*/c determined, the total-pressure-loss coefficient is computed according to equation (264) from the cascade geometry and a pertinent value of wake form factor H.

According to reference 156, for cascade measuring stations located more than about ½ chord length downstream of the blade trailing edge, the value of H will generally be less than about 1.2. For practical purposes, it was indicated that a constant value of H of about 1.1 can be used over a wide range of cascade configurations and incidence angles for measuring stations located between ½ and 1½ chord lengths behind the trailing edge. Loss coefficients based on inlet dynamic head can then be determined, if desired, from equation (266). The estimation of losses based on the diffusion factor D can, for example, produce a value of solidity that results in the least computed loss coefficient for a given velocity diagram.

The accuracy of the results obtained from the prediction procedure outlined is subject to the limitations and approximations involved in the diffusion analysis and wake momentum-thickness correlations. Strictly speaking, the procedure gives essentially a band of probable loss values at the cascade measuring station about ½ to 1½ chord lengths downstream of the blade trailing edge for the reference-incidence-angle setting and Reynolds numbers of about 2.5×10^5 and greater at low speed (up to about 0.3 inlet Mach number). It should also be noted at this point that the loss values obtained in this manner represent the low-speed profile loss of the cascade section. Such loss values are not generally representative of the losses of the section in a compressor blade row or in a high-speed cascade.

A corresponding loss-estimation technique for high Mach number flow is currently unavailable because of the unknown magnitude of the compressibility effect on the wake momentum-thickness ratio of a given cascade geometry. Furthermore, both the wake form factor H and the relation between θ^*/c and $\bar{\omega}$ (given for incompressible flow by eq. (264)) vary with Mach number. For example, if the velocity variation in each leg of the wake is assumed to vary according to the power relation

$$\frac{V}{V_0}=\left(\frac{y}{\delta}\right)^d \qquad (267)$$

where δ is the thickness of the wake and d is some constant, then variations of H and θ^* and of the relation between θ^*/c and $\bar{\omega}$ with outlet free-stream Mach number can be established analytically to illustrate the nature of the compressibility effects.

Curves of the variation of the ratios of compressible to incompressible form factor H/H_{inc} and momentum thickness θ^*/θ^*_{inc} with outlet Mach number for various d values obtained from numerical integration of the wake parameters involved are shown in figures 154 and 155. Recently, the increasing trend of H with M_2 was substantiated experimentally at the NACA Lewis laboratory in an investigation of the wake characteristic of a turbine nozzle (unpublished data). Curves of the ratio of the integrated value of $\bar{\omega}$ obtained from a given value of θ^*/c in a compressible flow to the value of $\bar{\omega}$ computed from the same value of θ^*/c according to the incompressible relation of equation (264) are shown in figure 156. It should be noted that for compressible flow the denominator in the loss-coefficient definition (eq. (263)) is now given by $P-p$.

In summary, therefore, an accurate prediction of the variation of reference total-pressure loss with inlet Mach number for a given cascade

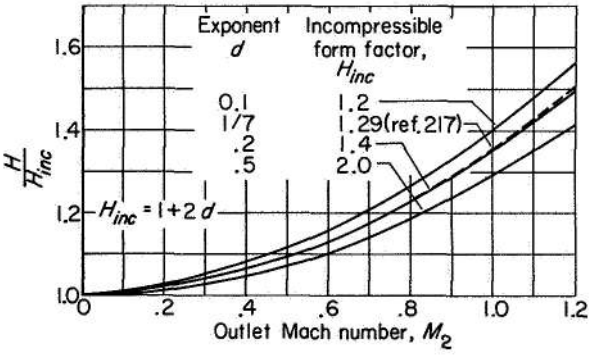

FIGURE 154.—Ratio of compressible to incompressible form factor for constant value of exponent in power velocity distribution.

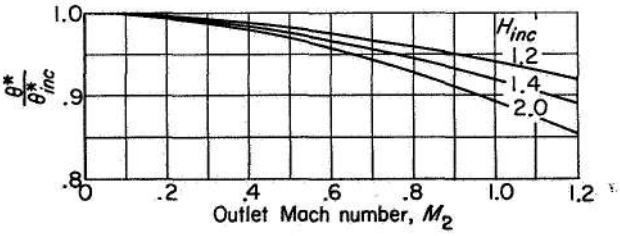

FIGURE 155.—Ratio of compressible to incompressible momentum thickness for constant full thickness and exponent for power velocity distribution.

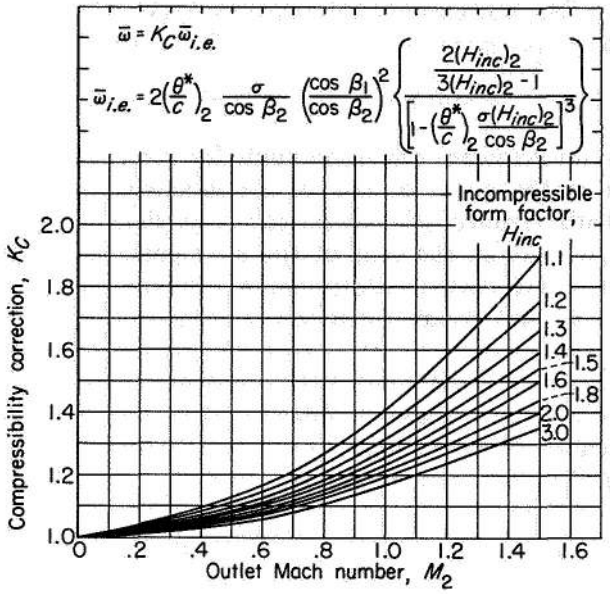

FIGURE 156.—Correction factor K_C for calculation of total-pressure-loss coefficient for compressible flow on basis of incompressible equation (264) as determined from model wake form with power velocity profile.

blade is currently impossible. At the moment, this pursuit is primarily an experimental one. Families of curves of wake momentum thickness and form factor against diffusion factor are required (with appropriate definitions for subsonic or supersonic flow) as in figure 146 or 148 for a wide range of inlet Mach number. Analytically, a simple compressible relation is needed between θ^*/c and $\bar{\omega}$ as a function of Mach number.

DEVIATION-ANGLE ANALYSIS

PRELIMINARY ANALYSIS

The correct determination of the outlet flow direction of a cascade blade element presents a problem, because the air is not discharged at the angle of the blade mean line at the trailing edge, but at some angle δ° to it (fig. 124). Since the flow deviation is an expression of the guidance capacity of the passage formed by adjacent blades, it is expected that the cascade geometry (camber, thickness, solidity, and chord angle) will be the principal influencing factor involved.

From cascade potential-flow theory (ref. 80, e.g.), it is found that the deviation angle increases with blade camber and chord angle and decreases with solidity. Weinig in reference 80 shows that the deviation angle varies linearly with camber for a given value of solidity and chord angle for infinitesimally thin blades at zero incidence. Furthermore, with deviation angle equal to zero at zero camber angle in this theory, it is possible to express the deviation angle as a ratio of the camber angle. Values of the ratio of deviation angle to camber angle for an infinitely thin circular-arc blade of small camber deduced from the theory of reference 80 are presented in figure 157 for a range of solidities and chord angles. The values in figure 157 are for the incidence angle for "impact-free entry" previously mentioned, which corresponds essentially to the condition of minimum loss.

The results of figure 157 show that, for a blade of zero thickness, the minimum-loss deviation angle is zero at zero camber angle. However, analysis indicates that this is not the case for blades of conventional thicknesses. A recent theoretical demonstration of the existence of a positive value of zero-camber deviation angle according to potential-flow calculations is given by Schlichting in reference 193. The computed variation of zero-camber deviation angle for a conventional 10-percent-thick profile at zero incidence angle as obtained in the reference is shown in figure 158.

It will be recalled from the discussion of the zero-camber minimum-loss incidence angle that, for the conventional staggered cascade ($0° < \gamma° < 90°$) with finite blade thickness set at zero incidence angle, a greater magnitude of velocity

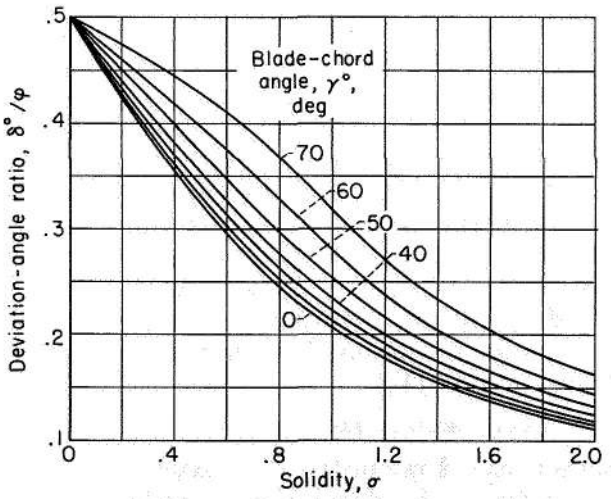

FIGURE 157.—Theoretical variation of deviation-angle ratio for infinitely thin circular-arc sections at "impact-free-entry" incidence angle according to potential theory of reference 80.

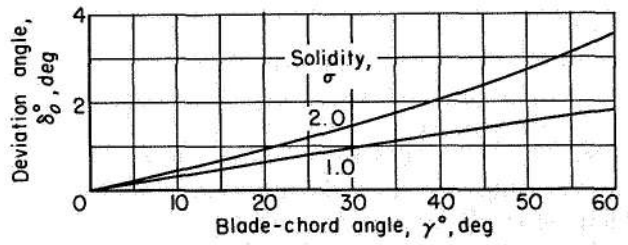

FIGURE 158.—Theoretical variation of deviation angle for conventional uncambered 10-percent-thick blade section at zero incidence angle as presented in reference 193.

occurs on the blade lower (concave) surface than on the upper (convex) surface (fig. 134). Such velocity distributions result in a negative blade circulation and consequently (as indicated by the solid vectors in fig. 159) in a positive deviation angle. Furthermore, since the deviation angle increases slightly with increasing incidence angle ($d\delta^\circ/di$ is positive in potential cascade flow), positive values of deviation angle will likewise be obtained at the condition of minimum-loss incidence angle (as illustrated by the dashed vectors in fig. 159). Since the zero-camber deviation angle arises from essentially a thickness blockage effect, the characteristics of the variation of minimum-loss zero-camber deviation angle with cascade geometry would be expected roughly to parallel the variation of the minimum-loss zero-camber incidence angle in figure 137. The low-speed reference-deviation-angle correlations may, therefore, involve intercept values as in the case of the reference-incidence-angle correlations.

In addition to the cascade-geometry factors mentioned, the low-speed deviation angles can also be affected by Reynolds number, turbulence, and Mach number. The thickened surface boundary layers resulting from low levels of Reynolds number and turbulence tend to increase the deviation angle. Variations in inlet Mach number can affect the deviation angle of a fixed two-dimensional-cascade geometry because of the associated changes in blade circulation, boundary-layer development, and outlet to inlet axial velocity ratio (compressibility effect on ρV_z).

DATA CORRELATIONS

Form of correlation.—Examination of deviation-angle data at reference incidence angle reveals that the observed data can be satisfactorily represented by a linear variation of reference deviation angle with camber angle for fixed solidity and air inlet angle. The variation of reference deviation angle can then be expressed in equation form as

$$\delta^\circ = \delta_o^\circ + m\varphi \tag{268}$$

where δ_o° is the reference deviation angle for zero camber, m is the slope of the deviation-angle variation with camber $(\delta^\circ - \delta_o^\circ)/\varphi$, and φ is the camber angle. As in the case of the analogous terms in the reference-incidence-angle relation (eq. (261)), δ_o° and m are functions of inlet-air angle and solidity.

The influence of solidity on the magnitude of the slope term m could also be directly included as a functional relation in equation (268), so that equation (268) could be expressed as

$$\frac{\delta^\circ - \delta_o^\circ}{\varphi} = \frac{m_{\sigma=1}}{\sigma^b} \tag{269}$$

where $m_{\sigma=1}$ represents the value of m (i.e., $(\delta^\circ - \delta_o^\circ)/\varphi$) at a solidity of 1, b is the solidity exponent (variable with air inlet angle), and the other terms are as before. It will be noted that equation (269) is similar in form to the frequently used deviation-angle rule for circular-arc blades originally established by Constant in reference 186 and later modified by Carter in reference 88. Carter's rule for the condition of nominal incidence angle is given by

$$\frac{\delta^\circ}{\varphi} = \frac{m_c}{\sqrt{\sigma}} \tag{270}$$

in which m_c is a function of blade-chord angle. Values of m_c determined from theoretical considerations for circular-arc and parabolic-arc mean lines (ref. 88) are shown in figure 160. In the

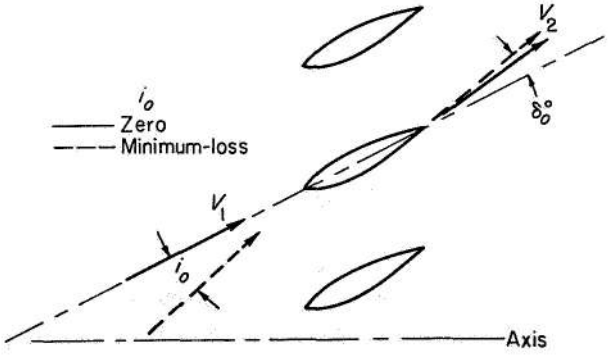

FIGURE 159.—Outlet flow direction for cascade of staggered uncambered blades.

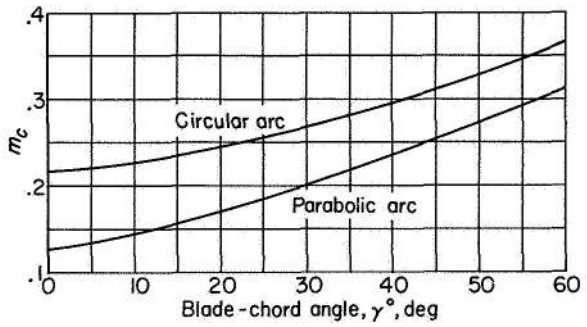

FIGURE 160.—Variation of factor m_c in Carter's deviation-angle rule (ref. 88).

ensuing correlations, both forms of the deviation-angle relation (eqs. (268) and (269)) are used, since each has a particular advantage. Equation (268), with m plotted as a function of β_1 and σ, is easier to use for prediction, especially if the calculation of a required camber angle is involved. Equation (269) may be better for extrapolation and for comparison with Carter's rule.

As in the case for the zero-camber reference minimum-loss incidence angle, the zero-camber deviation angle can be represented as a function of blade thickness as

$$\delta_o^\circ = (K_\delta)_{sh}(K_\delta)_t(\delta_o^\circ)_{10} \qquad (271)$$

where $(\delta_o^\circ)_{10}$ represents the basic variation for the 10-percent-thick 65-series thickness distribution, $(K_\delta)_{sh}$ represents any correction necessary for a blade shape with a thickness distribution different from that of the 65-series blade, and $(K_\delta)_t$ represents any correction necessary for maximum blade thicknesses other than 10 percent. (For a 10-percent-thick 65-series blade, $(K_\delta)_t$ and $(K_\delta)_{sh}$ are equal to 1.) The problem, therefore, is reduced to finding the values of m, b, and δ_o° (through eq. (271)) as functions of the pertinent variables involved for the various blade shapes considered.

NACA 65-(A_{10})-series blades.—From an examination of the plots of equivalent deviation angle against equivalent camber angle at reference minimum-loss incidence angle obtained from the cascade data, values of zero-camber deviation angle can be determined by extrapolation. The deduced plots of zero-camber deviation angle $(\delta_o^\circ)_{10}$ and slope term m as functions of solidity and air-inlet angle are presented in figures 161 and 162 for these blades. The subscript 10 indicates that the δ_o° values are for 10-percent maximum-thickness ratio. Values of the intercept term δ_o° and the slope term m were obtained by fitting a straight line to each data plot of reference equivalent deviation angle against equivalent camber angle for a fixed solidity and air inlet angle. The straight lines were selected so that both a satisfactory representation of the variation of the data points and a consistent variation for the resulting δ_o° and m values were obtained. The extrapolation of the values of m to $\beta_1=0$ was guided by the data for the 65-($12A_{10}$)10 blade at solidities of 1 and 1.5 reported in the cascade guide-vane investigation of reference 213 (for an aspect ratio of 1, as in ref. 39).

For the deviation-angle rule as given by equation (269), deduced values of $m_{\sigma=1}$ and exponent b as functions of inlet-air angle are presented in figures 163 and 164. The deduced rule values (eq. (268) or (269)) and the observed data points are compared in figure 165 to indicate the effectiveness of the deduced representations. The flagged symbols in the high-camber range in the figure represent blade configurations for which boundary-layer separation is indicated (D greater than about 0.62). In view of the higher loss levels for this condition, an increase in the magnitude of the deviation angle is to be expected compared with the values extrapolated from the smaller cambers for which a lower loss level existed.

C-Series circular-arc blades.—In view of the absence of systematic cascade data for the C-series circular-arc blade, an accurate determination of the rule constants cannot be made for this blade shape. However, a preliminary relation can be deduced on the basis of limited data. It appears that, for the uncambered C.4 section (ref. 192), if a value of $(K_\delta)_{sh}$ equal to 1.1 (as for the determination of i_0) is used, a satisfactory comparison between predicted and observed δ_o° values is obtained.

The characteristic number $m_{\sigma=1}$ in the deviation-angle design rule of equation (269) for a given blade mean line corresponds to the value of $(\delta_0-\delta_o^\circ)/\varphi$ at a solidity of unity. Cascade data for a C.4 circular-arc profile obtained from tunnels with good boundary-layer control are presented in references 167 (pt. I) and 199 for a solidity of 1.0 for $\beta_1=30°$, 42.5°, 45°, and 60°. Values of $(\delta_0-\delta_o^\circ)/\varphi$ were computed for these blades according to the δ_o° variations of figure 161. A value of $m_{\sigma=1}$ for $\beta_1=0°$ was obtained from the per-

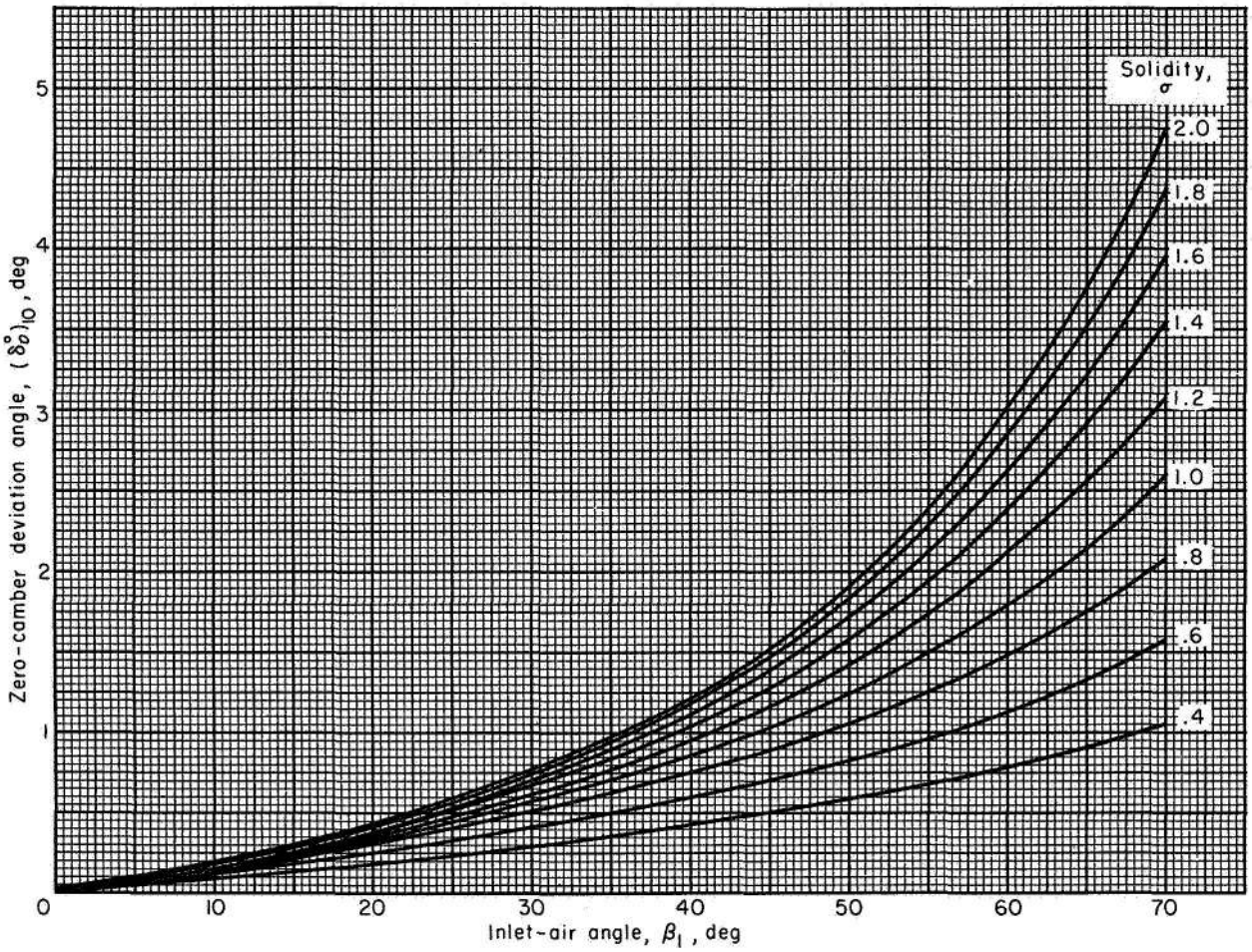

FIGURE 161.—Zero-camber deviation angle at reference minimum-loss incidence angle deduced from low-speed-cascade data for 10-percent-thick NACA 65-(A_{10})-series blades (ref. 39).

formance data of a free-stream circular-arc inlet guide vane presented in reference 214. These values of m are plotted in figure 166 against inlet-air angle, and the proposed variation of $m_{\sigma=1}$ for the circular-arc mean line is shown by the solid line.

In the absence of data covering a range of solidities, it is assumed that the solidity exponent b in the deviation-angle rule of equation (269) is independent of the profile shape and will therefore also be applicable for the circular-arc mean line. This assumption agrees with limited experimental data. The variation of ratio of deviation angle to camber angle obtained from constant-thickness circular-arc guide-vane sections of reference 215 ($\delta_0^\circ=0°$ for guide vanes) over a wide range of solidities is shown in figure 167. A computed variation based on values of b and $m_{\sigma=1}$ obtained from figures 164 and 166, respectively, is shown in the figure by the solid line. A satisfactory agreement with these circular-arc data is thus demonstrated for the value of b obtained from the 65-series data. On the basis of these results, deduced curves of m against $\beta 1$ for a range of solidities (for use in conjunction with eq. (268)) were computed for the C-series circular-arc blade as indicated in figure 168.

Double-circular-arc blades.—Although limited data are available for the double-circular-arc blade (refs. 40 and 197), it was felt that these data could not be reliably utilized in the construction of a deviation-angle rule because of the questionable two-dimensionality of the respective test tunnels. However, since the C-series and the double-

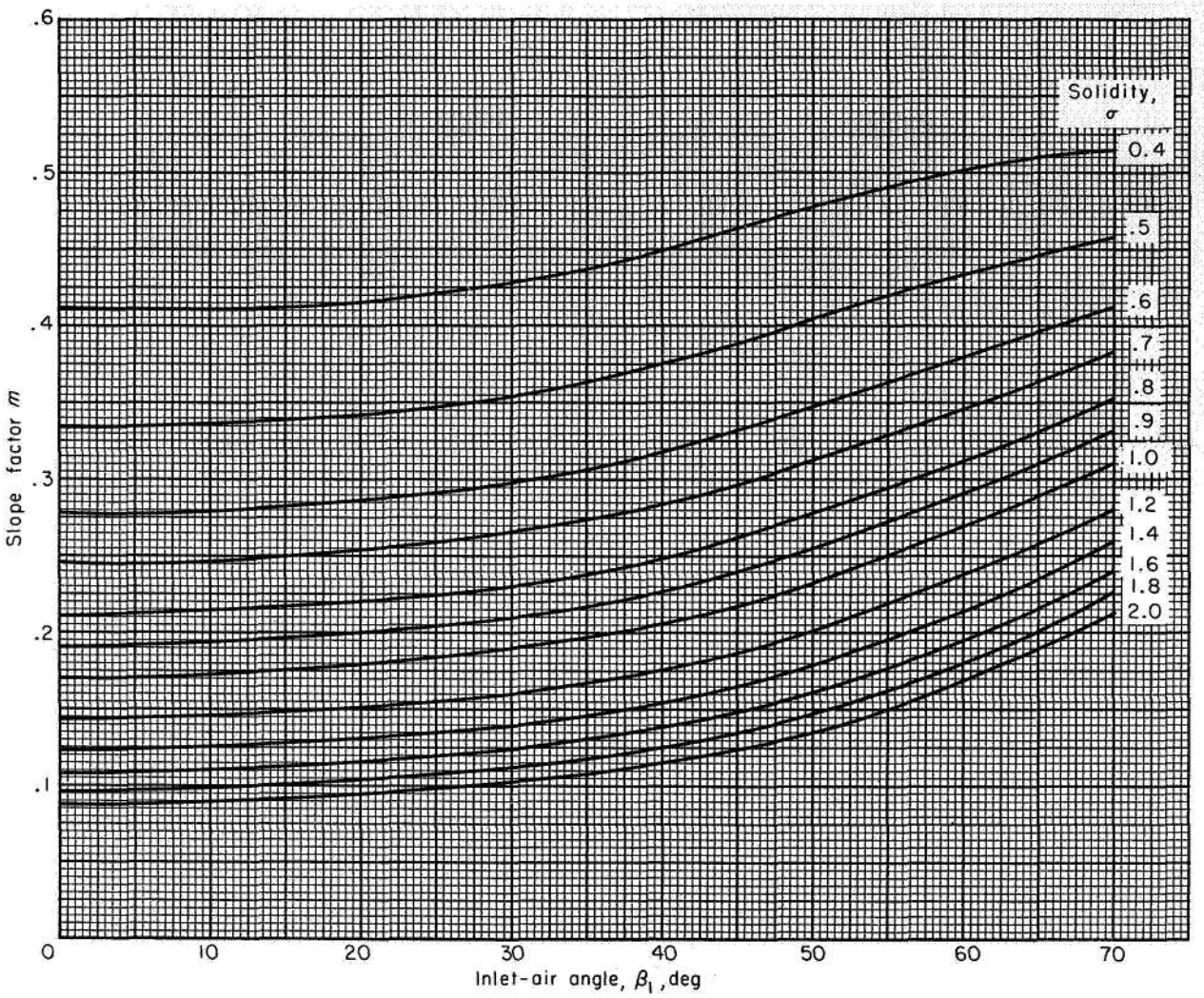

FIGURE 162.—Deduced variation of slope factor m in deviation-angle rule for NACA 65-(A_{10})-series blades as equivalent circular arc.

circular-arc blades differ only in thickness distribution, it is reasonable to expect that, as in the case of the reference-incidence-angle correlations, only the zero-camber deviation angles will be materially affected. Therefore, the slope-term value m deduced for the C-series circular-arc blade (fig. 168) might also be used for the double-circular-arc blade, but the δ_o° values may be different. An arbitrarily selected value of 0.7 for $(K_\delta)_{sh}$ in equation (271) (as for the reference-incidence-angle determination) is suggested for the double-circular-arc blade.

Comparison of rules.—In view of the widespread use of Carter's rule (eq. (270) with fig. 160) for predicting the deviation angle of circular-arc-mean-line blades, some results obtained from the use of Carter's rule were compared with the deduced rule of equation (269) with figures 161, 164, and 166. The principal difference between the two rules occurs in the blade orientation parameter used for the m variation and in the δ_o° and b variations. The value of the solidity exponent of ½ in equation (270) was originally obtained from limited data. Carter, in a later work (ref. 190), proposes a variable solidity exponent and indicates values close to 1 for accelerating cascades and close to ½ for decelerating cascades. The variation of b obtained from the NACA 65-(A_{10})-series blades

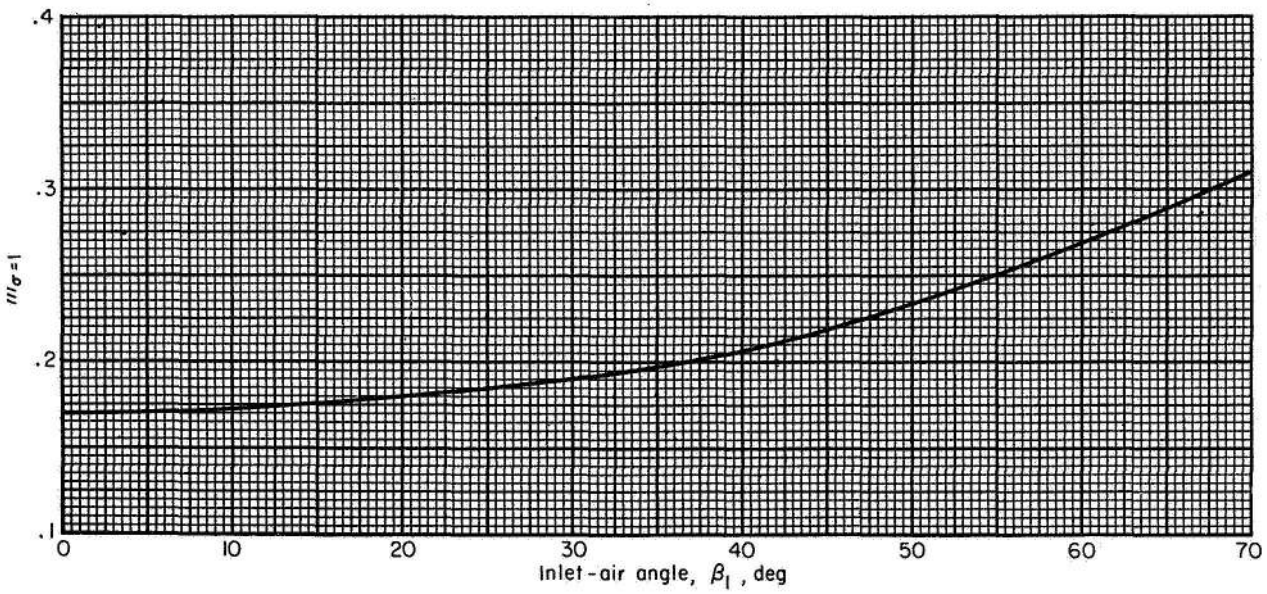

FIGURE 163.—Value of $m_{\sigma=1}$ in deviation-angle rule for 65-(A_{10})-series blades as equivalent circular arc (deduced from data of ref. 39).

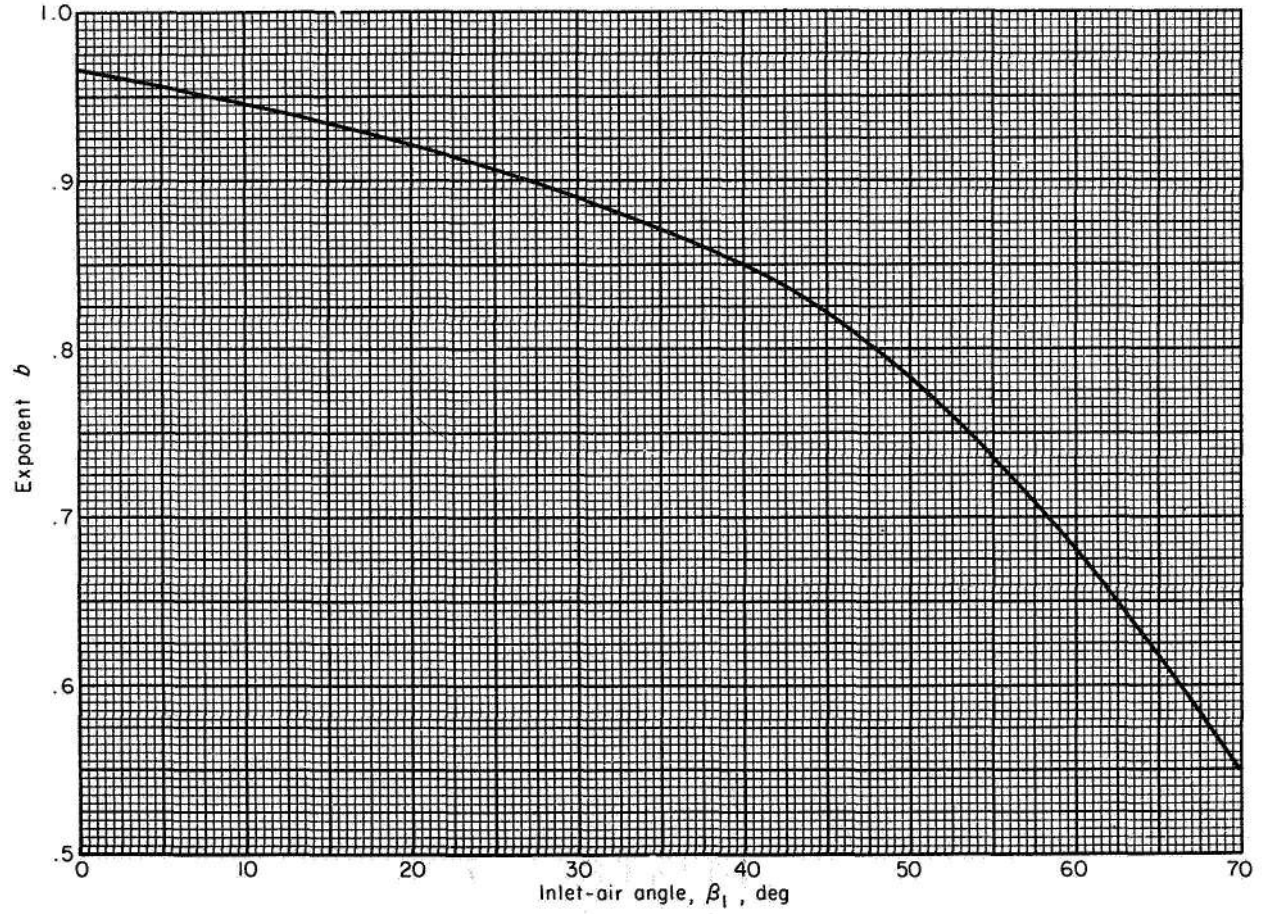

FIGURE 164.—Value of solidity exponent b in deviation-angle rule (eq. (269)) (deduced from data for 65-(A_{10})-series blades in ref. 39).

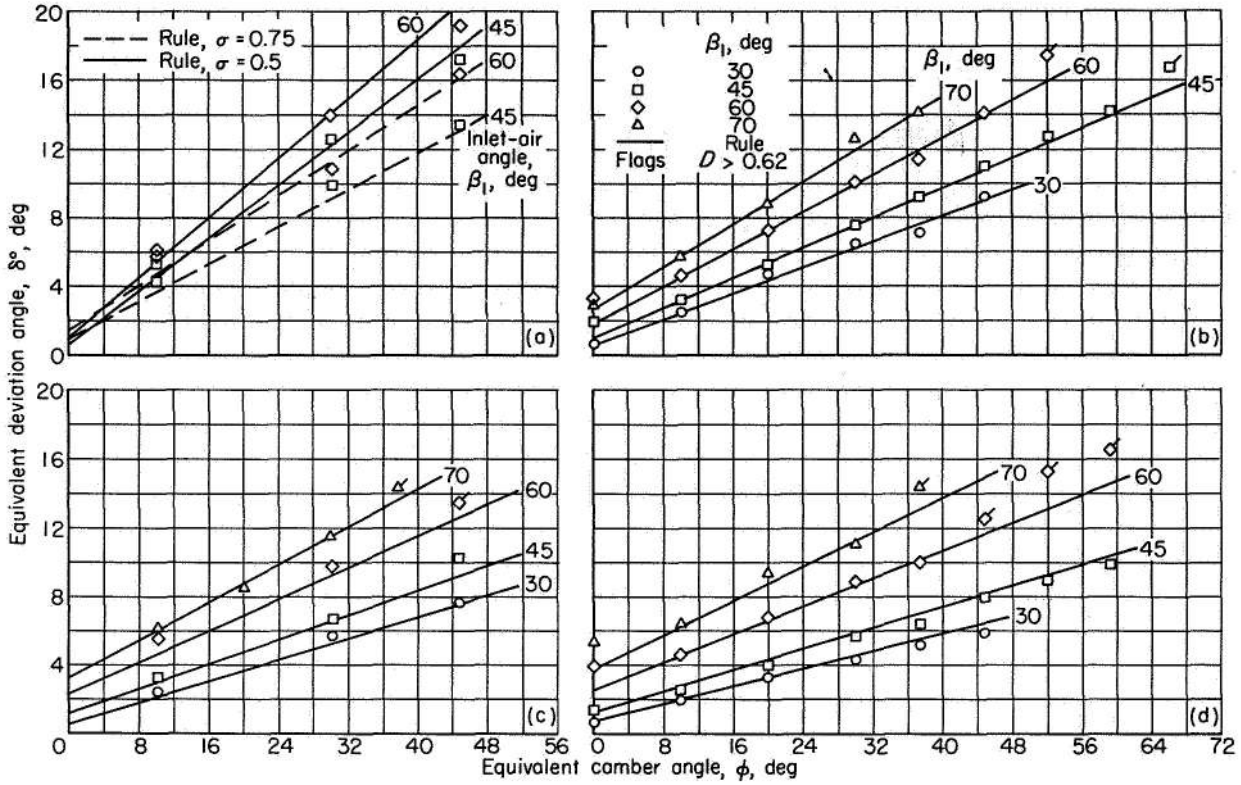

(a) Solidity, 0.5 and 0.75.
(b) Solidity, 1.0.
(c) Solidity, 1.25.
(d) Solidity, 1.5.

FIGURE 165.—Comparison between data values and deduced rule values of reference minimum-loss deviation angle for NACA 65-(A_{10})10-series blades as equivalent circular arc (data from ref. 39).

as equivalent circular arcs in figure 164 essentially confirms this trend. Actually, the deviation-angle rule in the form of equation (269) constitutes a modification of Carter's rule.

In addition to the basic differences between the rules in the magnitudes of the m, b, and δ_o° values, it is noted that Carter's rule was originally developed for the condition of nominal incidence angle, whereas the modified rule pertains to the reference minimum-loss incidence angle. However, since Carter's rule has frequently been used over a wide range of reference angle in its application, both rules were evaluated, for simplicity, for the reference minimum-loss incidence angle.

An illustrative comparison of predicted reference deviation angle as obtained from Carter's rule and the modified rule for a 10-percent-thick, thick-nosed circular-arc blade is shown by the calculated results in figure 169 for ranges of camber angle, solidity, and inlet-air angle. Deviation angles in figure 169 were restricted to cascade configurations producing values of diffusion factor less than 0.6. Blade-chord angle for Carter's rule was computed from the equation

$$\gamma^\circ = \beta_1 - i - \frac{\varphi}{2} \tag{272}$$

Reference incidence angle was determined from equations (261) and (262) and figures 137 and 138.

The plots of figure 169 show that, in practically all cases, the deviation angles given by the modified rule are somewhat greater in magnitude than those predicted by Carter's rule for the 10-percent-thick blade. This is particularly true for the high inlet-air angles. Thus, greater camber angles are required for a given turning angle according to the modified rule. Differences are even less for the double-circular, arc blade, as indicated in figure 170, since the δ_o° values are smaller for these blades. However, it should be kept in mind that the magnitude of the factors in the modified rule are proposed values based on limited data. Further research is required to establish the modified rule on a firmer foundation.

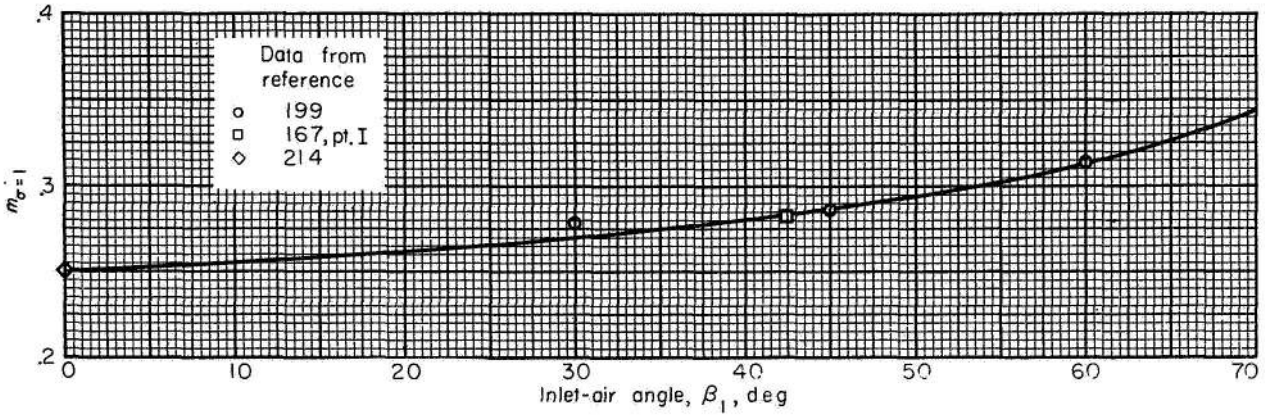

FIGURE 166.—Deduced values of $m_{\sigma=1}$ for circular-arc mean line.

Effect of blade maximum thickness.—Available data on the variation of reference deviation angle with blade maximum-thickness ratio obtained from cascade investigations of the 65-($12A_{10}$) blade of reference 202 are shown in figure 171. The solid symbols representing the values of deviation angle at zero thickness were determined by subtracting the values of $(\delta_o^\circ)_{10}$ obtained from figure 161 from the measured value of deviation angle at 10-percent maximum thickness obtained from the data in figure 171. A very reasonable variation with thickness ratio, as indicated by the faired curves, is thus obtained for all three configurations. The increasing slope of the deviation-angle variation with increasing thickness ratio is believed due to some extent to the accompanying increase in wake losses.

Preliminary values of a correction factor for maximum-thickness ratio $(K_\delta)_t$ deduced from the data of figure 171 are shown in figure 172. In the absence of further data, it is proposed that this correction curve is also applicable to other conventional blade shapes.

Effect of Reynolds number.—In view of the large rise in loss as blade-chord Reynolds number is reduced (fig. 152), a corresponding rise in deviation angle (or decrease in turning angle) is to be expected. Experimental confirmation of the marked effect of Reynolds number on blade deviation angle at fixed incidence angle is illustrated in figure 173 for several compressor blade shapes. The variation of deviation angle with Reynolds number over a range of incidence angle is demonstrated in figure 174. In all cases the variation of the deviation or turning angle closely parallels

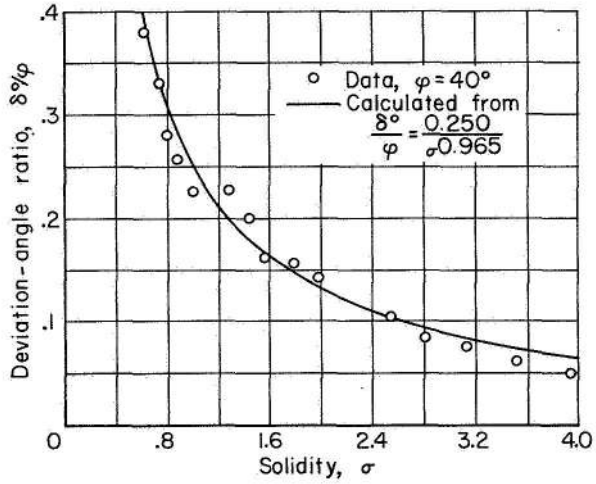

FIGURE 167.—Comparison of experimental deviation-angle ratio and rule values using solidity exponent given by figure 164. Data for circular-arc inlet guide vanes in annular cascade (ref. 215).

the variation of the loss. Therefore, factors involved in the deviation-angle variation are the same as those for the loss behavior. Correspondingly, no Reynolds number correction factors that will be applicable for all blade configurations have been established. The deduced deviation-angle rule developed herein is applicable at Reynolds numbers of about 2.5×10^5 and greater.

Effect of inlet Mach number.—Experimental variations of minimum-loss deviation angle with inlet Mach number are presented in figure 175 for two circular-arc blades. Further cascade data in terms of air-turning angle at fixed angle of attack are shown in figure 176 for two other compressor blade shapes. (Since the data in fig. 176 were

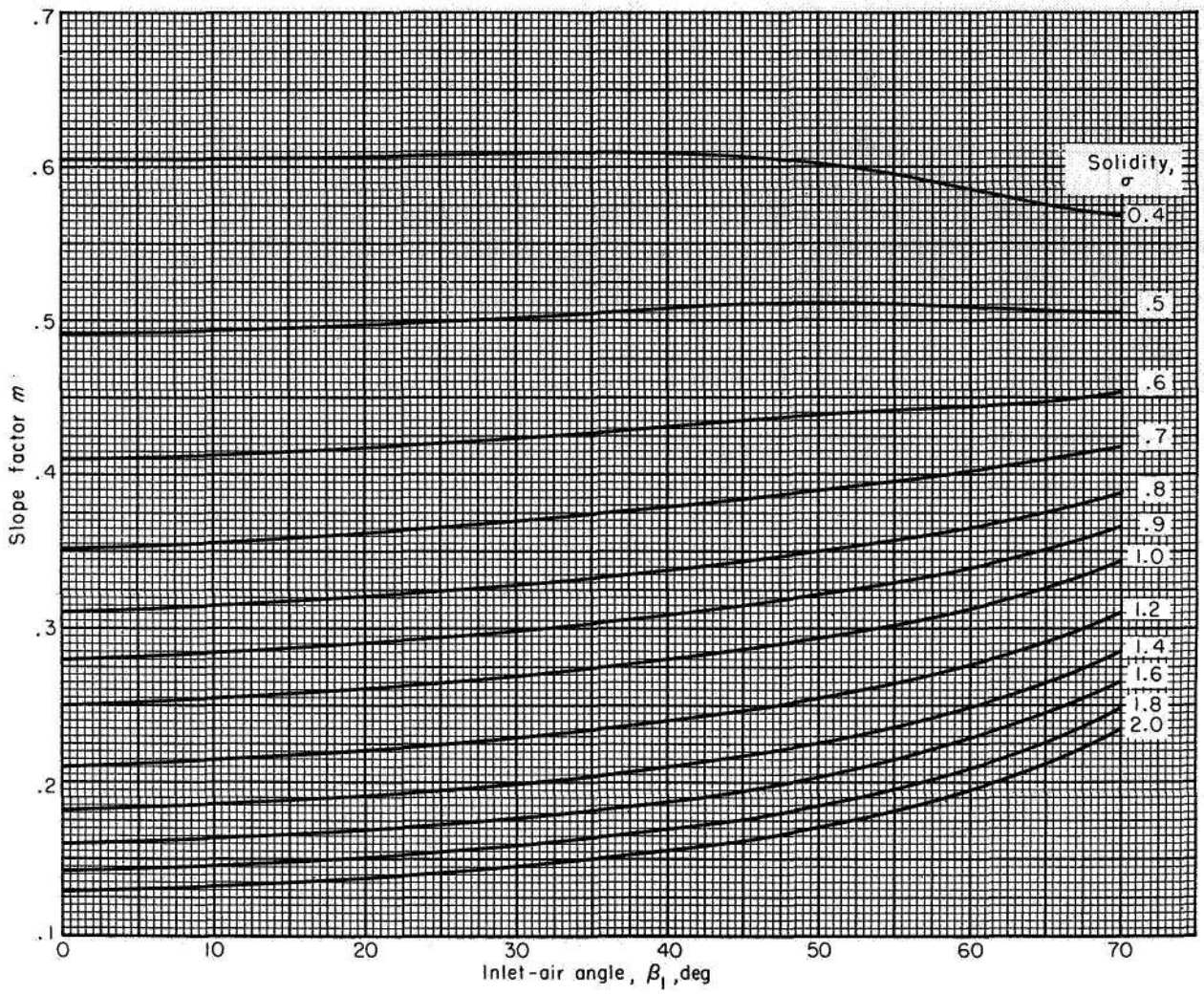

FIGURE 168.—Deduced variation of slope factor m in deviation-angle rule (eq. (268)) for circular-arc-mean-line blades.

obtained at constant angle of attack, the variation of turning angle is an inverse reflection of the variation of deviation angle.) The data of figures 175 and 176 indicate that deviation angle varies little with inlet Mach number up to the limiting value. As indicated in the Preliminary Analysis section, the resultant Mach number effect for a given blade configuration will depend on the relative magnitude of the various factors involved. Apparently, the net effect is small up to the limiting value of inlet Mach number. Large increases in deviation angle can be expected, however, when the loss rises rapidly at the limiting Mach number because of the adverse effects of the shock formation. (The rise in deviation angle in the data is always associated with the sharp rise in loss.)

Variation with incidence angle.—Thus far, of necessity, the analysis has been conducted for flow conditions at only one reference position on the general curve of loss against incidence angle. Ultimately, of course, it is desired to predict flow variations over the entire range of incidence angle. The variation of deviation angle with incidence angle for a fixed geometry in the two-dimensional cascade is primarily a function of the change in the guidance capacity of the cascade arising from the change in orientation of the approaching flow (a potential-flow effect) and of the variation in the wake loss. Since no information

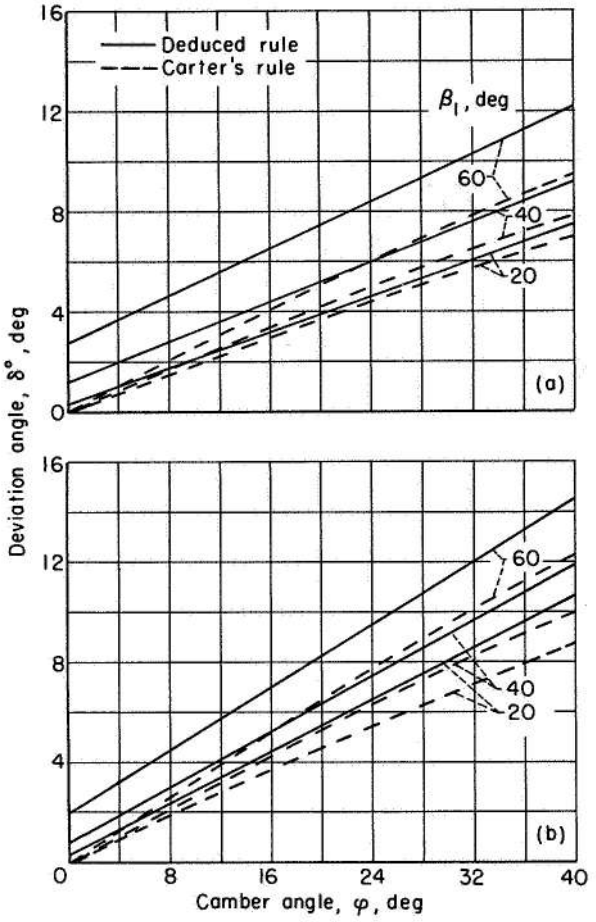

(a) Solidity, 1.5.
(b) Solidity, 1.0.

FIGURE 169.—Comparison of calculated reference deviation angles according to Carter's rule and deduced modified rule for 10-percent-thick, thick-nose circular-arc blades.

is currently available on the effect of losses, attention is centered on deviation-angle variations in the region of low loss, where the trend of variation approaches that of the potential flow.

Examination of potential-flow theory (Weinig, ref. 80, e.g.) shows that a positive slope of deviation angle against incidence angle exists (i.e., deviation angle increases with incidence angle). Calculations based on the theory of Weinig reveal that the magnitude of the slope varies with solidity and blade-chord angle. The deviation-angle slope approaches zero for infinite solidity (deviation angle is essentially constant at high solidity) and increases as solidity is reduced. At

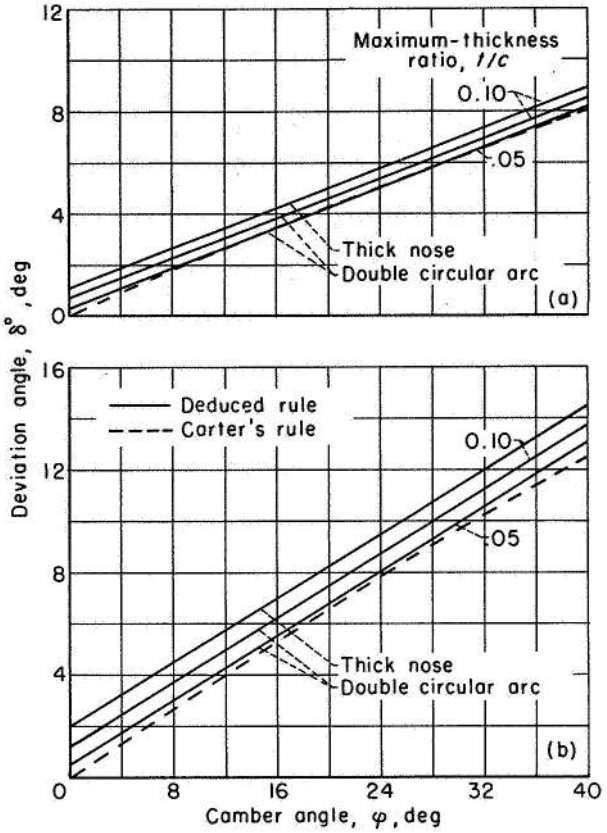

(a) Solidity, 1.5; inlet-air angle, 40°.
(b) Solidity, 1.0; inlet-air angle, 60°.

FIGURE 170.—Comparison of calculated reference deviation angles according to Carter's rule and deduced modified rule for circular-arc blades of different thickness.

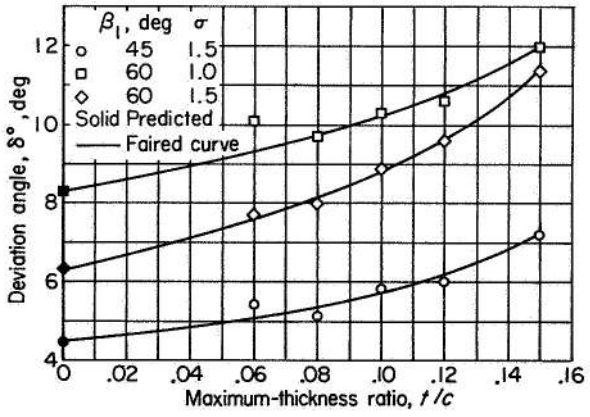

FIGURE 171.—Variation of deviation angle with blade maximum-thickness ratio for NACA 65-($12A_{10}$) blade in region of minimum loss (data from ref. 202).

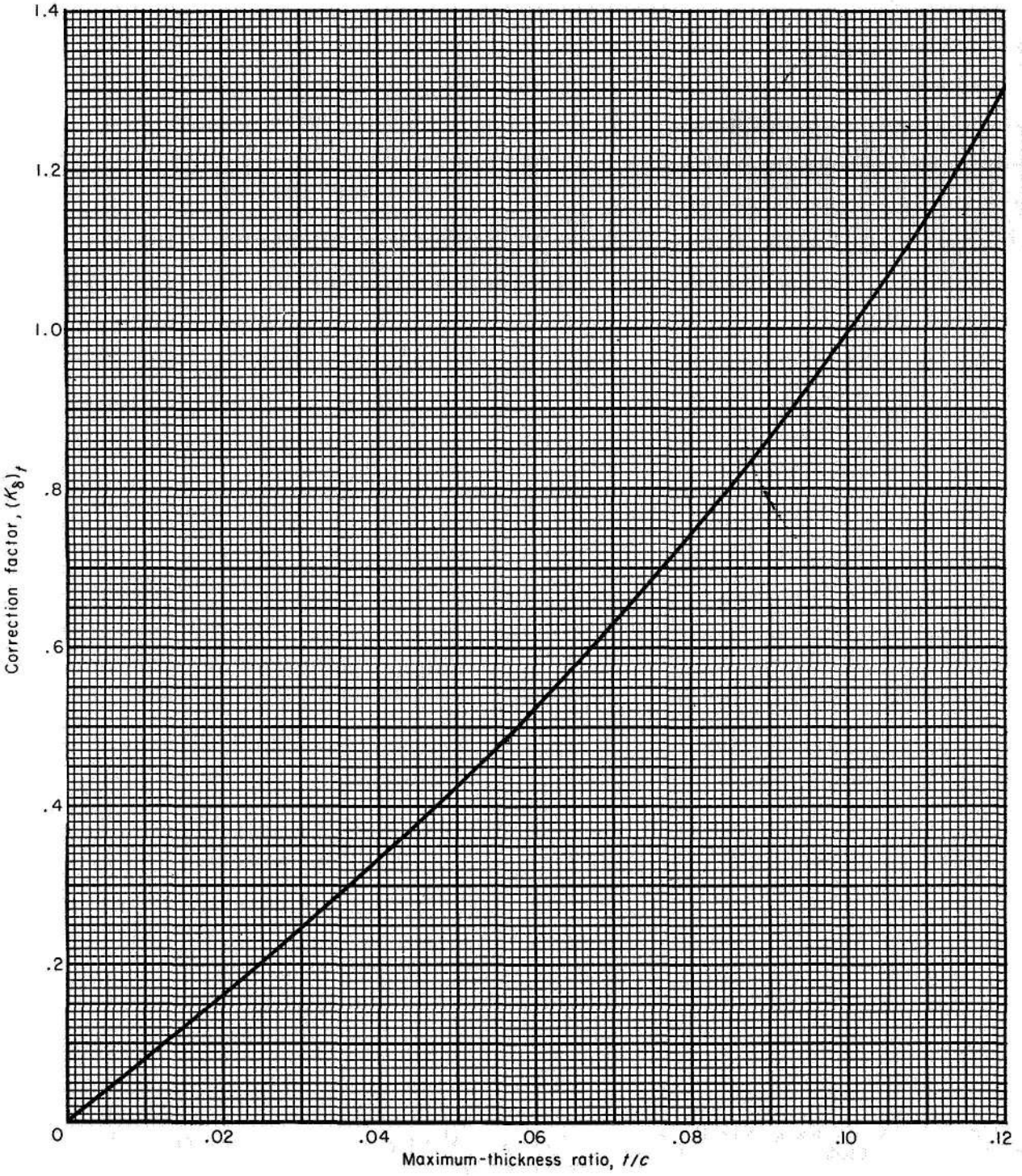

FIGURE 172.—Deduced maximum-thickness correction for zero-camber reference minimum-loss deviation angle (eq. (271)).

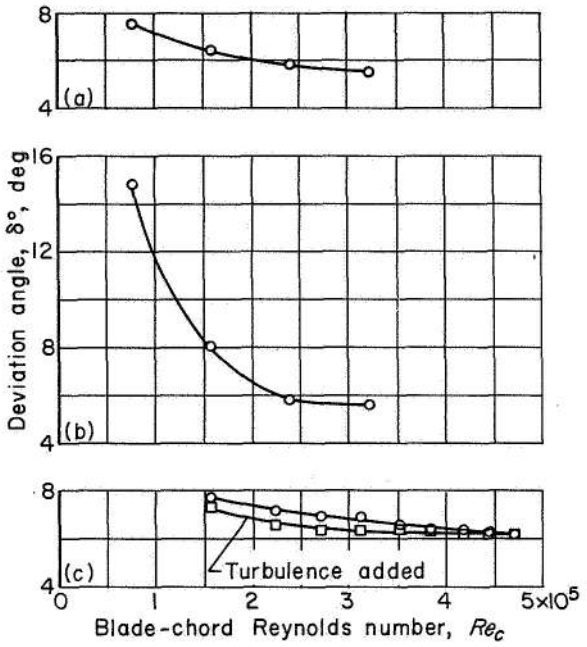

(a) 10C4/25C50 blade. Solidity, 1.33; blade-chord angle, 42.5° (ref. 40).
(b) 10.5 2A/25C50 blade. Solidity, 1.33; blade-chord angle, 42.5° (ref. 40).
(c) NACA 65–(12)10 blade. Solidity, 1.5; inlet-air angle, 45° (ref. 39).

FIGURE 173.—Illustrative variations of reference deviation angle with Reynolds number.

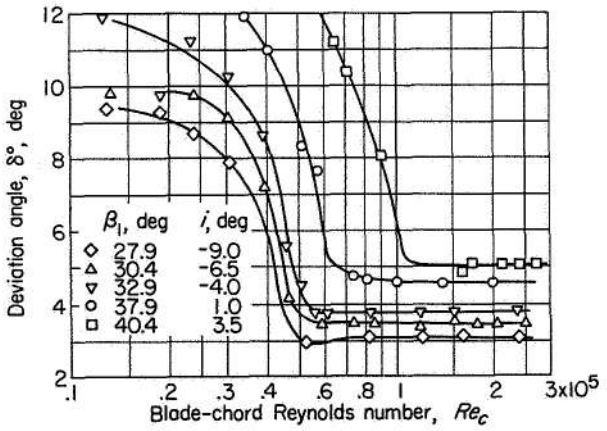

FIGURE 174.—Variation of deviation angle with Reynolds number for 10C4/40 P40 blade. Solidity, 1.33 (ref. 183).

constant solidity, the slope of deviation angle against incidence angle increases as the chord angle is increased. These trends indicate physically that the greater the initial guidance effect

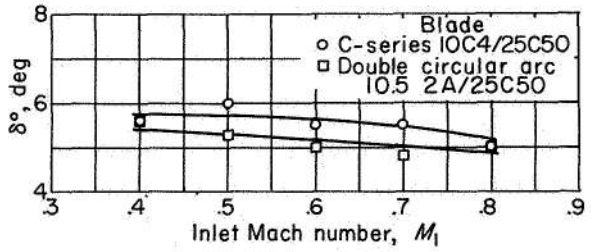

FIGURE 175.—Variation of reference deviation angle with inlet Mach number for circular-arc blades. Solidity, 1.333; blade-chord angle, 42.5° (ref. 40).

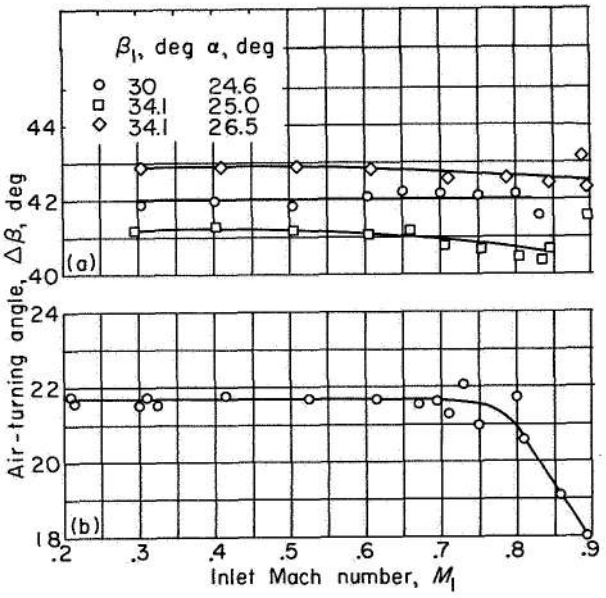

(a) T1(18A_6I_{45})08 blade. Solidity, 1.5 (ref. 207).
(b) 65–(12A_{10})10 blade. Solidity, 1.0; inlet-air angle, 45°; angle of attack, 16.5° (ref. 122).

FIGURE 176.—Variation of air-turning angle with inlet Mach number in region of minimum loss.

(high solidity and low blade angle), the less sensitive the deviation angle is to changes in incidence angle.

For analysis purposes, since the region of low loss is generally small, the variation of deviation angle with incidence angle for a given cascade geometry in the region of minimum loss can be represented as

$$\delta^\circ = \delta^\circ_{ref} + (i - i_{ref}) \left(\frac{d\delta^\circ}{di}\right)_{ref} \qquad (273)$$

where $(d\delta^\circ/di)_{ref}$ represents the slope of the deviation-angle variation at the reference incidence

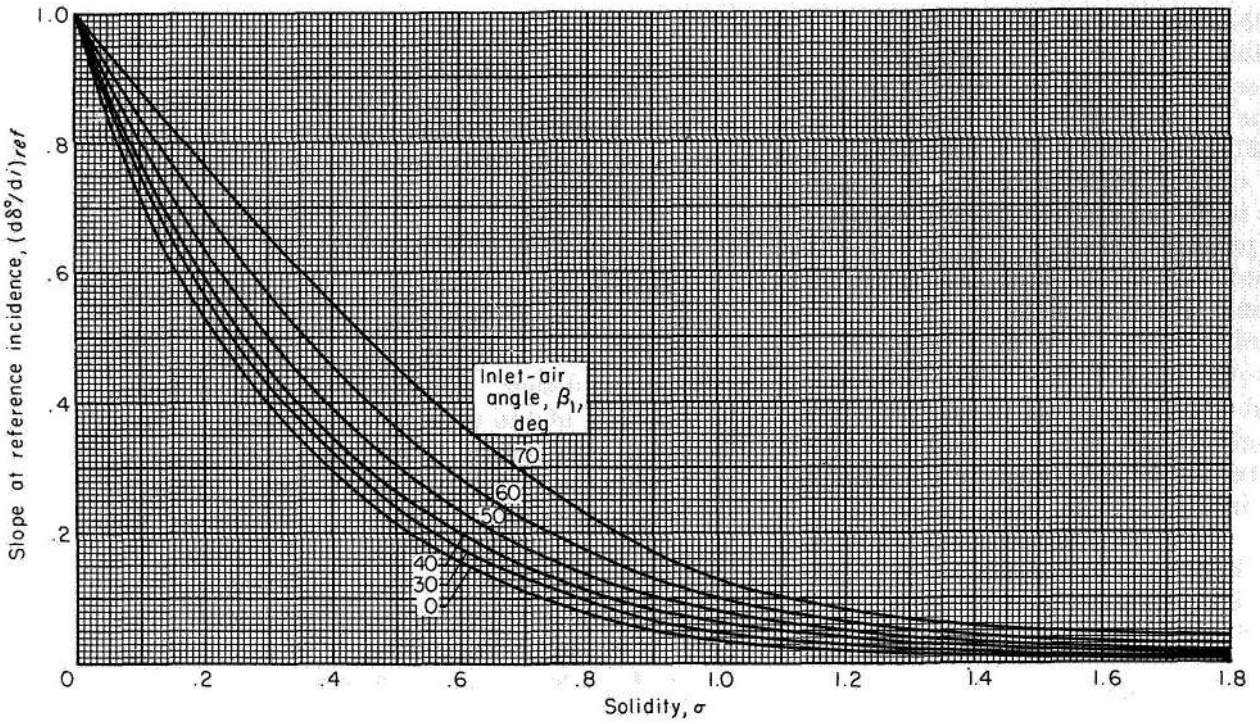

FIGURE 177.—Deviation-angle slope $d\delta°/di$ at reference incidence angle deduced from low-speed data for NACA 65-(A_{10})10 blades (ref. 39).

angle. An empirical determination of the magnitude of the slope of the variation of deviation angle with incidence angle was obtained from an analysis of the low-speed experimental data for the 65-(A_{10})10 blades of reference 39. From the plot of deviation angle against incidence angle for each configuration (as in fig. 127, e.g.), the slope of the curve at the minimum-loss incidence angle was evaluated graphically. The deduced variation of reference slope magnitude $d\delta°/di$ obtained from fairings of these values is presented in figure 177 as a function of solidity and inlet-air angle. Qualitative agreement with theory is strongly indicated by the data. Since the phenomenon is essentially a guidance or channel effect, it is anticipated that the slope values of figure 177 will also be applicable for other conventional blade shapes. Thus, it is possible to predict the deviation angle at incidence angles other than the reference location within the low-loss range of operation from the use of equation (273) and figure 177.

SUMMARY

The analysis of blade-section deviation angle shows that the variation of reference deviation angle with cascade geometry at low speed can be satisfactorily established in terms of an intercept value $\delta_0°$ and a slope value m as given by equation (268). The experimental data could also be expressed in terms of a rule similar in form to Carter's rule, as indicated by equation (269). Deduced values of $\delta_0°$ and m were obtained as a function of β_1 and σ from the data for the 10-percent-thick 65-(A_{10})-series blades of reference 39 as equivalent circular arc (figs. 161 and 162). Rules for predicting the reference deviation angle of the C-series and double-circular-arc blades were also deduced based on the correlations for the 65-(A_{10})-series blades and on limited data for the circular-arc blade (figs. 161 and 168).

The procedure involved in estimating the low-speed reference deviation angle of a blade section is as follows: From known values of β_1 and σ, $(\delta_0°)_{10}$ is selected from figure 161, and m is selected from figure 162 for the 65-(A_{10})-series blades or from figure 168 for circular-arc-mean-line blades. The value of $(K_\delta)_t$ for the blade maximum-thickness ratio is obtained from figure 172, and the approximate value of $(K_\delta)_{sh}$ is selected for the type of thickness distribution.

For the 65-series blades, $(K_\delta)_{sh}=1.0$, and it is proposed that $(K_\delta)_{sh}$ be taken as 1.1 for the C-series blades and as 0.7 for the double-circular-arc blade. The value of δ_o° is then computed from equation (271), and finally δ° is determined from the blade camber angle according to equation (268). As in the case of reference i_o values, the use of the proposed values of $(K_\delta)_{sh}$ is not critical for good accuracy in the final determination of δ°. Reference deviation angle can also be computed according to the rule in the form of equation (269) in conjunction with figures 163, 164, and 166.

The camber angle required to produce a given turning angle at the reference condition at low speed can readily be calculated by means of the preceding incidence-angle and deviation-angle correlations when the inlet-air angle and blade solidity are known. From equations (57), (261), and (268), the camber angle as a function of the turning, deviation, and incidence angle is

$$\varphi=\frac{\Delta\beta-(i_o-\delta_o^\circ)}{1-m+n} \tag{274}$$

or, in terms of the thickness corrections (eqs. (262) and (271)),

$$\varphi=\frac{\Delta\beta-[(K_t)_{sh}(K_t)_t(i_o)_{10}-(K_\delta)_{sh}(K_\delta)_t(\delta_o^\circ)_{10}]}{1-m+n} \tag{275}$$

For simplicity, since $(K_t)_{sh}=(K_\delta)_{sh}=K_{sh}$, equation (275) can be expressed in the form

$$\varphi=\frac{\Delta\beta-K_{sh}\overline{K}_t[(i_o)_{10}-(\delta_o^\circ)_{10}]}{1-m+n} \tag{276}$$

where $\overline{K}_t$ represents some correction factor for blade thickness, such that

$$\overline{K}_t[(i_o)_{10}-(\delta_o^\circ)_{10}]\cong(K_t)_t(i_o)_{10}-(K_\delta)_t(\delta_o^\circ)_{10} \tag{277}$$

Curves of the values of $(i_o)_{10}-(\delta_o^\circ)_{10}$ as a function of β_1 and σ are given in figure 178; curves of the values of $1-m+n$ as a function of β_1 and σ are given in figure 179(a) for the 65-(A_{10})-series mean line and in figure 179(b) for the circular-arc mean line; and values of $\overline{K}_t$ are plotted as a function of β_1 and t/c in figure 180. The use of the chart values of $\overline{K}_t$ in equation (276) gives results within about 0.1° of the exact values given by equation (275). Required camber angle can thus be determined readily by equation (276) in conjunction with figures 178 to 180.

CONCLUDING REMARKS

The foregoing analysis has presented a correlation of available two-dimensional experimental cascade data in terms of parameters significant in compressor design. The work essentially presents a summary of the state of experimental cascade research with regard to cascade performance at the reference incidence angle. Rules and procedures were evolved for the prediction of the magnitude of the reference total-pressure loss and the reference incidence and deviation angles in satisfactory agreement with existing cascade data. The rules may also be of help in reducing the necessary experimental effort in the accumulation of further cascade data.

However, the present analysis is incomplete. Many areas, such as the deviation-angle rule for the double-circular-arc blade, require further data to substantiate the correlations. Furthermore, additional information concerning the influence of high Mach number and off-design incidence angles of cascade performance is needed.

Finally, it is recognized that the performance of a given blade geometry in the compressor configuration will differ from the performance established in the two-dimensional cascade. These differences result from the effects of the various three-dimensional phenomena that occur in compressor blade rows. It is believed, however, that a firm foundation in two-dimensional-cascade flow constitutes an important step toward the complete understanding of the compressor flow. The extent to which cascade-flow performance can be successfully utilized in compressor design can only be established from further comparative evaluations. Such comparisons between observed compressor performance and predicted two-dimensional-cascade performance on the basis of the rules derived herein are presented in chapter VII.

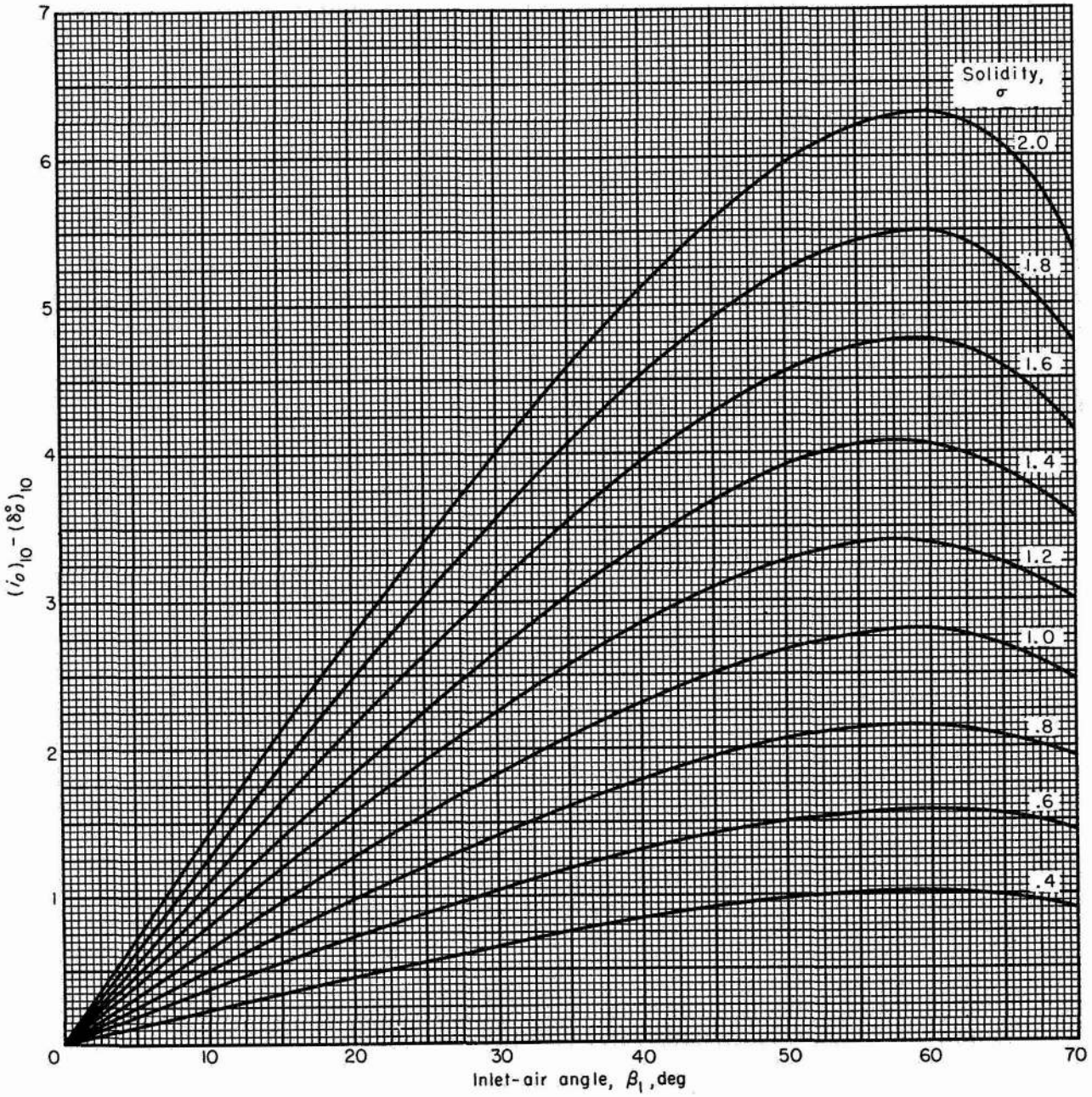

FIGURE 178.—Variation of $(i_o)_{10}-(\delta_o^*)_{10}$ with inlet-air angle and solidity (eq. (276)).

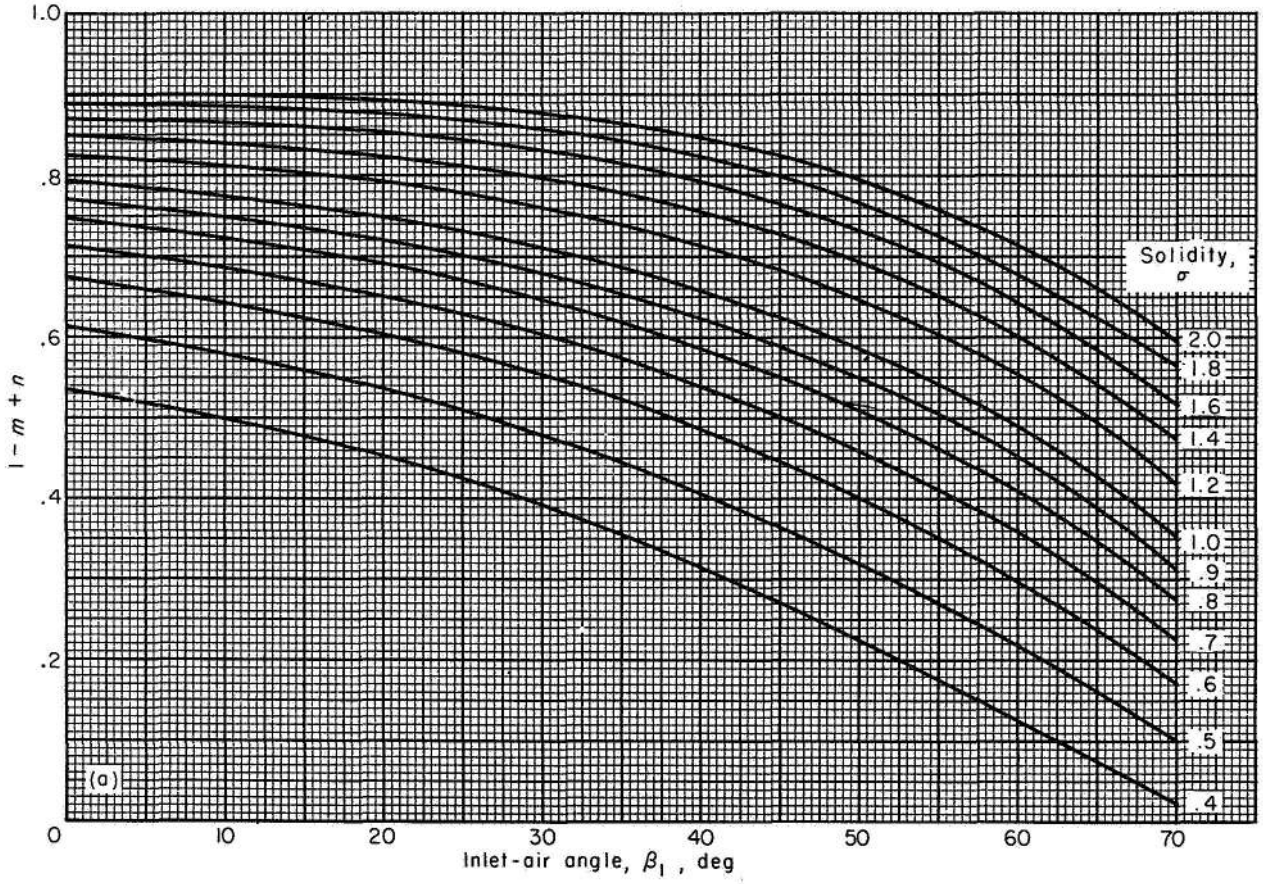

(a) NACA 65-(A_{10})-series blades as equivalent circular arc (eq. (276))

FIGURE 179.—Variation of $1-m+n$.

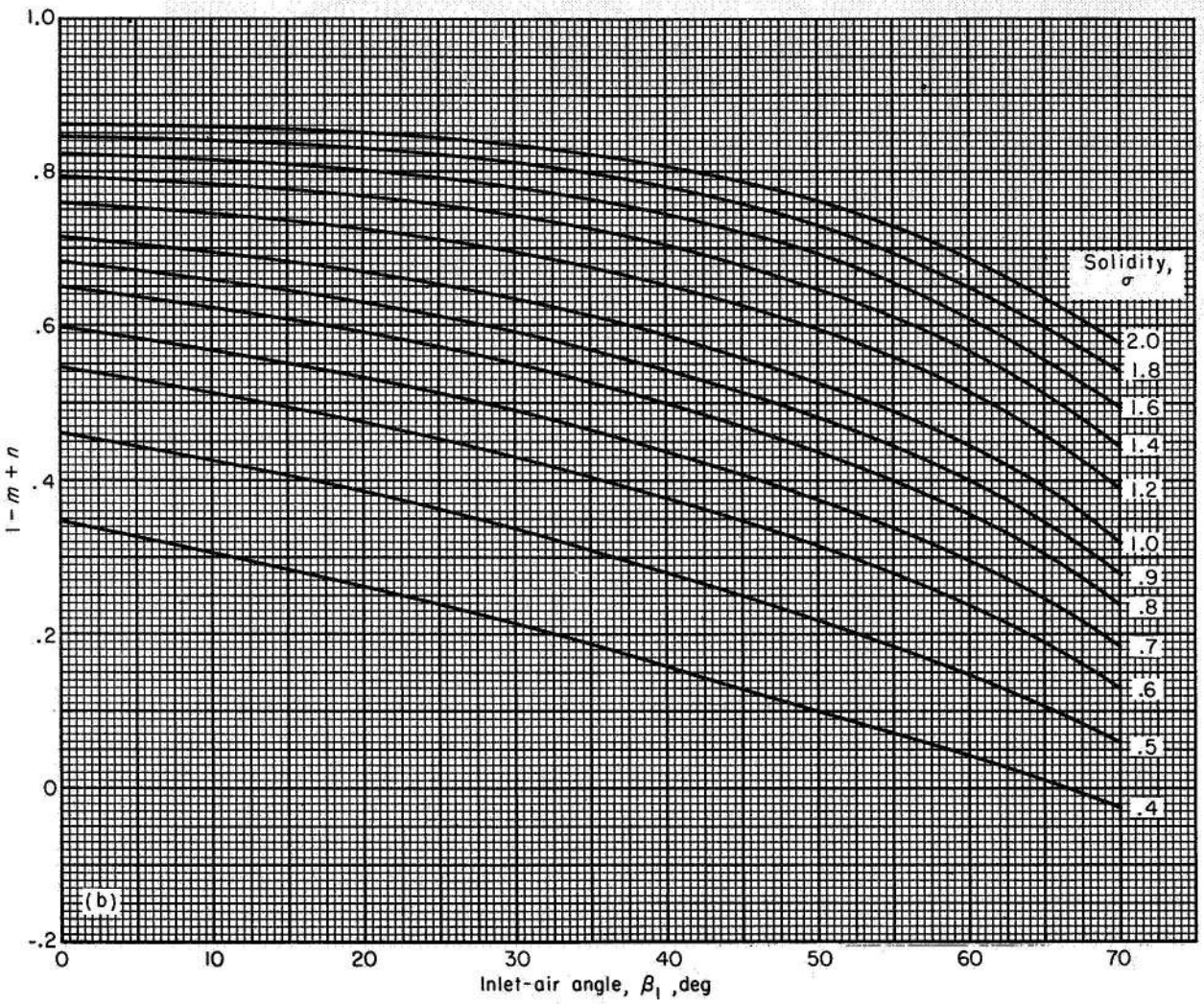

(b) Circular-arc-mean-line blades (eq. (276))

FIGURE 179.—Concluded. Variation of $1-m+n$.

691-564 O-65-16

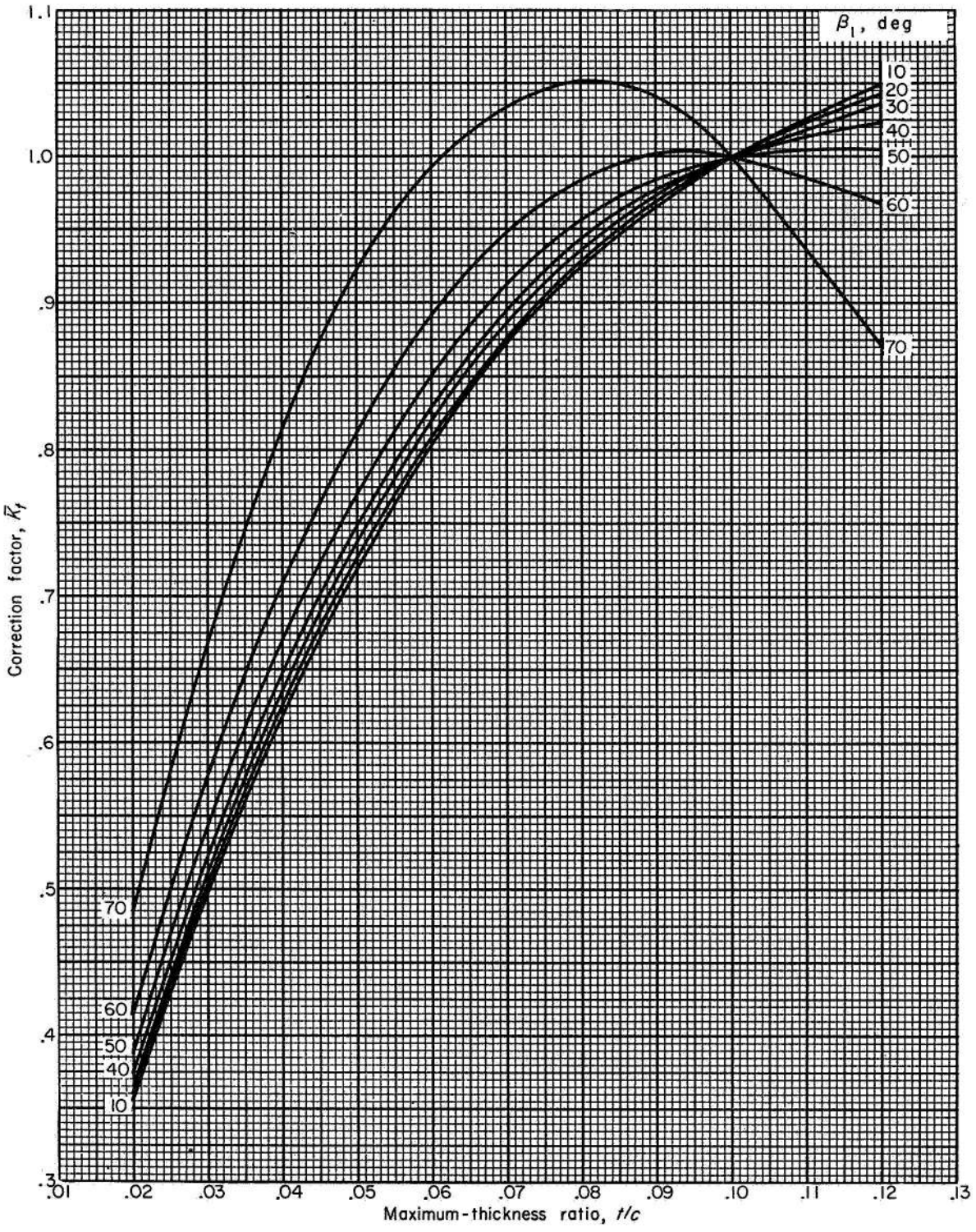

FIGURE 180.—Variation of thickness-correction factor $\overline{K}_t$ for camber calculation (eq. (276)).